

From Reliability to Security: How RIS-Assisted Adaptive SM and SSK Enhances Wireless Systems

Chaorong Zhang, Benjamin K. Ng, Ke Wang, Hui Xu, and Chan-Tong Lam

Abstract—This paper proposes two novel wireless transmission schemes, namely reconfigurable intelligent surface (RIS)-assisted received adaptive spatial modulation (RASM) scheme and RIS-assisted received adaptive space shift keying (RASSK) scheme, designed to enhance spectral efficiency (SE) and physical layer security (PLS). In both proposed schemes, transmitting bits are dynamically mapped at receive antennas by leveraging the characteristics of the RIS in each time slot, which enables the enhancement of signal-to-noise ratio (SNR) at specific selected antennas with nearly few power, thus leading to a reliable and green wireless communication. Unlike conventional fixed-antenna RIS-RSM/GSSK, the term “adaptive” indicates the number of active antennas dynamically changes per symbol, conveying extra spatial information to break existing spectral efficiency bottlenecks. This adaptive approach facilitates the conveyance of extra bits to the receiver, which means it needs less cost of radio-frequency chains at transmitter while improving SE. Besides, the proposed schemes offer an inherent PLS security advantage, as the eavesdropper is unable to completely detect signals reflected from the RIS. To comprehensively evaluate the performance of the proposed RASM and RASSK schemes, this paper presents a detailed analytical performance of their spectral efficiency, detection complexity, bit error rate, and secrecy rate, which are accompanied by insightful findings and conclusions. Simulation and analytical results demonstrate the superiority of the proposed schemes, showcasing their improved error performance and robustness against wiretapping, while also highlighting the potential of the RASM and RASSK schemes for future wireless applications.

Index Terms—RIS, IM, spectral efficiency, PLS

I. INTRODUCTION

A. Index Modulation

With the exponential growth of devices accessing wireless networks, communication throughput and data rates have surged recently. In response, novel techniques have emerged, with index modulation (IM) standing out. Numerous variants exist in the IM area. Prominent multi-antenna techniques include spatial modulation (SM), space shift keying (SSK), generalized space shift keying (GSSK), and others. These traditional schemes map antenna indices to convey information: single-antenna activation in SM/SSK and multi-antenna combinations in generalized schemes, enabling extra bits and enhancing spectral efficiency (SE) [1]. In IM schemes, constellation symbols modulated by M -ary phase shift keying (PSK) or quadrature amplitude modulation (QAM) are transmitted, while additional bits are encoded via antenna indices, each representing distinct transmitted bits. Unlike SM, SSK omits M -ary symbols, reducing digital modulation complexity at transmitter and receiver. As noted in [2], SSK exhibits slightly better bit-error-rate (BER) performance than SM with perfect channel state information (CSI) at the receiver. However,

conventional SSK [2] demands numerous antennas for higher SE, raising costs and degrading BER. GSSK, introduced in [3], alleviates antenna costs by activating a fixed number, but yields inferior BER compared to SM and SSK. Thus, another groundbreaking IM approach is called adaptive spatial modulation (ASM), which provides flexibility through variable activated transmit antennas forming diverse antenna combinations (ACs), achieving superior SE over traditional SM, SSK, etc. [4]. By minimizing transmit antennas or ACs, ASM’s BER outperforms other IM schemes at equivalent SE. ASM incorporates constellation symbols, increasing complexity relative to adaptive space shift keying (ASSK), which excludes them. To lower the processing complexity at transmitter, this paper also explores ASSK, based on SSK principles where antennas emit pure power, simplifying modulation. As a trade-off, ASM and ASSK enhance SE beyond traditional IM schemes but introduce challenges, such as elevated radio frequency (RF) chain costs and physical layer security (PLS) concerns. To address these, a novel technique is applied to ASM and ASSK for system improvement.

B. Reconfigurable Intelligent Surface

As a promising technique garnering considerable attention in recent years, reconfigurable intelligent surfaces (RIS) holds great potential for application in future beyond 5th generation (5G) and 6th generation (6G) wireless communication systems. The RIS comprises a chip, referred to as the intelligent unit, which is connected to the transmitter. This intelligent unit receives information about phase adjustments and subsequently controls the angles of the reflection elements (REs) accordingly [5]. The REs, as fabricated from the special materials that can reflect electromagnetic waves [6], are arranged in a two-dimensional (2D) planar array [7] and can be individually controlled by the intelligent unit. According to it, a deployment feature in the RIS is provided, that is, an extension in coverage of wireless communication through altering the communication delivery into the desired directions [8]. Recently, the state-of-the-art applications of RIS have expanded profoundly, integrating advanced architectures, such as multi-layer refracting and self-powered absorptive surfaces, into complex space-air-ground integrated networks and satellite-terrestrial systems to fundamentally boost both coverage reliability and endogenous physical layer security [9], [10], [11], [12]. Unlike the traditional relays, the RF chains and amplifiers are not required in the RIS, which can better improve the power utilization in communication. Therefore, through the RIS, the phase shift of transmitted signals can be adjusted with near few powers and the signal-to-noise ratio

(SNR) can be further enlarged at receiver, which is named the passive beamforming [13]. By possessing these advantages, the RIS can achieve the IM scheme at receive antennas by adjusting the phase to achieve the passive beamforming at one or more specific antennas, in which it can more effectively address the aforementioned issues of the ASM and ASSK schemes mentioned above and provides a viable consideration of system design for the proposed scheme, as illustrated as follows.

C. RIS-assisted IM schemes

Given extensive research on reconfigurable intelligent surfaces (RIS), IM is increasingly integrated into its applications. First, RIS acts as a passive relay to enhance IM communication quality. In [14]-[15], an RIS-assisted IM scheme is proposed where SSK operates at transmit antennas, improving BER performance via RIS assistance, as termed TSSK herein for convenience. RIS-assisted SM schemes are explored in various state-of-the-art works [16]-[20], with SM at transmit antennas and RIS boosting receiver SNR, so-called the TSM in this paper. To reduce antennas, RIS-assisted GSSK is introduced in [16], adhering to GSSK activation principles at transmit antennas, though with inferior BER compared to TSSK and TSM. Recent advancements include diverse RIS-assisted IM variants operable not only at transmitters but also at receivers via antenna selection, referred to as received IM herein. As a trade-off in RIS-assisted systems, received IM offers advantages like superior BER, reduced transmitter complexity, and potential gains in SE over related schemes [21]-[25]. In [21], RIS-assisted RSM and RSSK are first proposed with antenna selection at receive antennas, yielding good BER but omitting transmitter-RIS channel due to AP design, with room for SE improvement. Subsequently, RIS-assisted RGSM and RGSSK schemes emerge in [22]-[23], enhancing SE via novel low-complexity detectors, albeit with poorer BER than RSM and RSSK. All these schemes employ fixed selected or activated antennas for information mapping, limiting flexible SE enhancement or dynamic antenna adjustment. To overcome this, we propose two novel schemes with a flexible adaptive antenna selection algorithm, enabling dynamic resource configuration for improved SE adaptability and surpassing fixed-antenna constraints. While our proposed schemes rely on coherent detection, acquiring the requisite cascaded CSI typically requires dedicated pilot-based training protocols. To circumvent this estimation overhead, non-coherent transmission designs present a promising alternative [26], [27], [28], which demonstrate significant potential in reducing system complexity while enhancing secure communications. Unlike classic SM/SSK that requires multiple power-hungry transmit RF chains and relies on random fading, receive-side RIS-IM uses a single-antenna transmitter and a RIS to artificially reshape the channel. This paradigm minimizes IoT transmitter costs and enhances security. Advancing this, our schemes introduce an adaptive receive-antenna activation mechanism, fundamentally breaking the SE bottlenecks of conventional fixed-antenna RIS-IM. Besides, differing from traditional received IM schemes that rely on a fixed number of active antennas and physically deactivate the rest, our proposed schemes keep all receive antennas active

and utilize RIS passive beamforming to dynamically vary the number of selected antennas per time slot. This adaptive mechanism fundamentally breaks the SE bottlenecks of fixed-antenna designs while intrinsically avoiding the computational overhead of complex real-time channel optimization. The RIS-assisted transmitted ASM scheme is termed TASM, with ASM at the transmitter.

D. Contributions

The existing RIS-assisted IM schemes still face several critical challenges, e.g., contradicting with the low-cost nature of wireless communications to multiple RF chains, limit SE adaptability in dynamic channels by fixing antenna activation patterns, low PLS in wireless applications, etc. To address these issues, we propose two novel RIS-assisted received IM schemes, termed the RIS-assisted received ASM (RASM) and RIS-assisted RASSK schemes, which dynamically map information bits to receive ACs instead of transmit antennas. Note that prior works on RIS-assisted IM schemes primarily focus on BER or data rate, overlooking the potential of RIS to enhance PLS in this domain. By leveraging RIS's passive beamforming to enhance SNR at selected receive ACs, our schemes achieve higher SE, while the unique design in reflections inherently enhances the physical layer security against eavesdropping. Overall, the main contributions of this work can be briefly summarized as follows:

- This paper proposes two novel RIS-assisted IM schemes, denoted as RASM and RASSK, which enhance performance metrics such as BER, spectral efficiency, secrecy rate (SR), and robustness by first employing adaptive antenna selection at the receive antennas and leveraging the RIS to boost the SNR at the receiver.
- In our schemes, eavesdroppers face challenges in reconstructing transmitted signal due to the inherent security mechanism embedded in the dynamic receive-side mapping. This paper pioneers the theoretical analysis of the SR for these schemes under a passive eavesdropper, bridging the gap in PLS-based studies for RIS-assisted IM schemes.
- Accounting for side lobes and inevitable interference, the REs are partitioned into constructive and non-constructive components in our schemes with detailed analytical performance. Also, to further reduce the complexity of the proposed schemes, a generalized pre-defined ACs selection at the receiver is designed.
- This work presents Monte Carlo simulations of the proposed schemes, evaluating BER, SE, and secrecy rate under perfect and imperfect CSI scenarios with artificial noise (AN), ML and maximal ratio combining (MRC) detectors, yielding valuable insights.

E. Organization and Notation

Organization: The rest of the paper is organized as follows: In Sec. II, the system model of the RASM and RASSK schemes with introduction of detection is given. Sec. III provides the illustration of random ACs selection. The analytical performance of SE, BER performance, and detection complexity is presented in Sec. IV. Sec. V provides the system model of the RASM and RASSK schemes with the eavesdropper and

the analytical performance in PLS of the proposed schemes by deriving SR. The theoretical and simulation results of the RASM and RASSK schemes and other related schemes with different conditions are shown in Sec. VI. Eventually, the conclusion is given in Sec. VII.

Notation: Boldface letter is used to denote the matrices. $(\cdot)^T$ and $(\cdot)^H$ denote the transpose and complex conjugate transpose operations. $\text{diag}(\cdot)$ represents diagonal matrix operation. $\mathbb{C}^{n \times m}$ is the space of $n \times m$ complex-valued matrices. The real part of a complex variable can be denoted as $\Re\{\cdot\}$. $P_r(\cdot)$ represents the probability of an event. The exponential function is denoted by both $\exp(\cdot)$ and $e^{(\cdot)}$, which, while distinct in notation, convey the identical mathematical concept. $Q(\cdot)$ means the Q-function. $\|\cdot\|_2$ is the second-norm operation, while $\mathbb{E}(\cdot)$ stands for statistical expectation operation. $j \triangleq \sqrt{-1}$ is the imaginary number. $f(\cdot)$ and $f(\cdot|\cdot)$ denote the probability density function (PDF) the conditional PDF. $\mathbb{E}(\cdot)$ represents the operation of expectation. $\binom{n}{k}$ stands for the binomial coefficient from n choose k . $\mathcal{CN}(\mu, \sigma^2)$ represents the complex Gaussian distribution with mean μ and variance σ^2 . $\mathbb{D}(\cdot)$ stand for variance operations.

II. SYSTEM MODEL

A. Configuration and Wireless Channel

1) *Applied Scenarios:* This section illustrates the system models for the proposed RIS-assisted received IM schemes, RASM and RASSK, to enhance wireless networks. As depicted in Fig. 1, we consider a SIMO uplink in an IoT scenario where fixed sensors collect environmental data¹, e.g., temperature, and transmit it to a base station (BS). The sensor employs a single transmit antenna ($N_t = 1$), while the BS has N_r receive antennas. Due to obstructions, the direct link is blocked, relying solely on the RIS path. The RIS comprises N REs and an intelligent unit linked to the transmitter. For instance, in the RASM scheme, bit sequence 010 maps to an AC selecting the first and fourth receive antennas; the intelligent unit directs the first RE subset to amplify the signal toward the first antenna and the second subset toward the fourth. Note that RASM transmits M -ary constellation symbols, whereas RASSK conveys only pure power, necessitating more receive antennas in RASSK. We denote N_r^1 for RASM and N_r^2 for RASSK, with $N_r^1 \ll N_r^2$.

2) *Rayleigh Channel Fading:* In both system models, the channel matrix of the channel from the transmitter to the receiver is defined as $\mathbf{H}_1 \in \mathbb{C}^{N \times 1}$, the other from the RIS to the receiver is represented as $\mathbf{H}_2 \in \mathbb{C}^{N_r \times N}$, which both follow the Rayleigh flat fading with zero mean value and unit variance. The diagonal matrix of adjusted phase in the RIS can be given as $\Phi = \text{diag}(\exp(j\varphi_{1,m}), \exp(j\varphi_{2,m}), \dots, \exp(j\varphi_{N,m}))$, with $\varphi_{i,m}$ representing the adjusted phase shift of i -th reflecting element and for m -th receive antenna. Furthermore, we define the wireless channel from the transmit antenna to the i -th reflecting element and the one from the i -th reflected to the m -th receive antenna as h_1^i and $h_2^{i,m}$ with $i = 1, 2, \dots, N$ and

$m = 1, 2, \dots, N_r$, respectively. h_1^i and $h_2^{i,m}$ are assumed to be independent and identically distributed complex Gaussian random variables with $\mathcal{CN}(0, 1)$, which can be extended to $h_1^i = \alpha_i e^{-j\theta_i}$ and $h_2^{i,m} = \beta_{i,m} e^{-j\omega_{i,m}}$, with α and β representing the Rayleigh factors in various channels, as well θ and ω representing the phase shift of these three channels.

3) *Specific Antenna Settings:* For convenience, we define the receive antenna activation vector for the r -th AC as $\mathbf{v}_r = [v_{r,1}, v_{r,2}, \dots, v_{r,N_r}]^T \in \{0, 1\}^{N_r \times 1}$, where $v_{r,n} = 1$ indicates that the n -th receive antenna is selected, and $v_{r,n} = 0$ otherwise. For example, based on the mapping table in Fig. 1, if the transmitted bit sequence is ‘001’, the second and third antennas are activated. The corresponding receive antenna vector is thus denoted as $\mathbf{v}_2 = [0, 1, 1, 0]^T$. The number of active antennas in each AC, denoted as N_a ($1 \leq N_a \leq N_r$), dynamically changes within each symbol period. For instance, as shown in Fig. 1, $N_a = 1$ is employed to transmit the bit sequence ‘000’, whereas $N_a = 2$ is utilized for the sequences ‘001’ and ‘010’. This dynamic activation mechanism significantly enhances the flexibility of antenna configurations and substantially improves the SE. The full set of permissible ACs is defined as \mathcal{A} , containing J possible combinations. Consequently, the total number of ACs can be expressed as $J = \sum_{n=1}^{N_r} \binom{N_r}{n} = 2^{N_r} - 1$. Following the principle of the proposed adaptive scheme, although N_r receive antennas are deployed, a dynamically varying subset of N_a antennas is selected to convey the spatial information.

4) *Working Principle:* The REs are evenly divided into N_a parts, which has $N_E = \lfloor \frac{N}{N_a} \rfloor$ number of REs, and each part is corresponding for one selected receive antenna to achieve the passive beamforming.² Besides, each antenna not only can receive the signals reflected from the REs that are corresponding for itself but also from the non-corresponding ones. Specifically, as shown in Fig.1, the first receive antenna can receive the signals reflected from the REs corresponding for itself (as shown in the red dashed line) and can be affected by those for the fourth receive antenna (as shown in blue dashed line) in the meanwhile, which leads to the constructive part and non-constructive part in the signals for m -th receive antenna, respectively. Notably, all N_r receive antennas remain active during transmission, unlike traditional activation-based IM where unselected antennas are deactivated. Instead, the RIS employs passive beamforming to focus gain through constructive reflections on selected antennas while imposing non-constructive interference on others. The RE allocation strategy involves sequential assignment based on the sorted order of selected receive antenna indices in the AC, pre-agreed upon by transmitter and receiver. As shown in the mapping table in Fig. 1, for bit sequence 010 (mapping to antennas 1 and 4), the first RE part amplifies the signal toward antenna 1, and the second toward antenna 4. Similarly, for 100 (mapping to antennas 1, 2, and 3), the first part targets antenna 1, the second antenna 2, and the third antenna 3. This sequential

²This even division strategy for RE allocation ensures fair resource distribution without real-time optimization. It enables straightforward passive beamforming by assigning equal RE subsets to boost SNR at each selected antenna. The method reduces computational overhead at the intelligent unit, suiting dynamic IoT scenarios with limited processing power.

¹Since both transmit sensors and the receive BS are fixed in this scenario, mobility-induced channel fluctuations are beyond the scope of this paper.

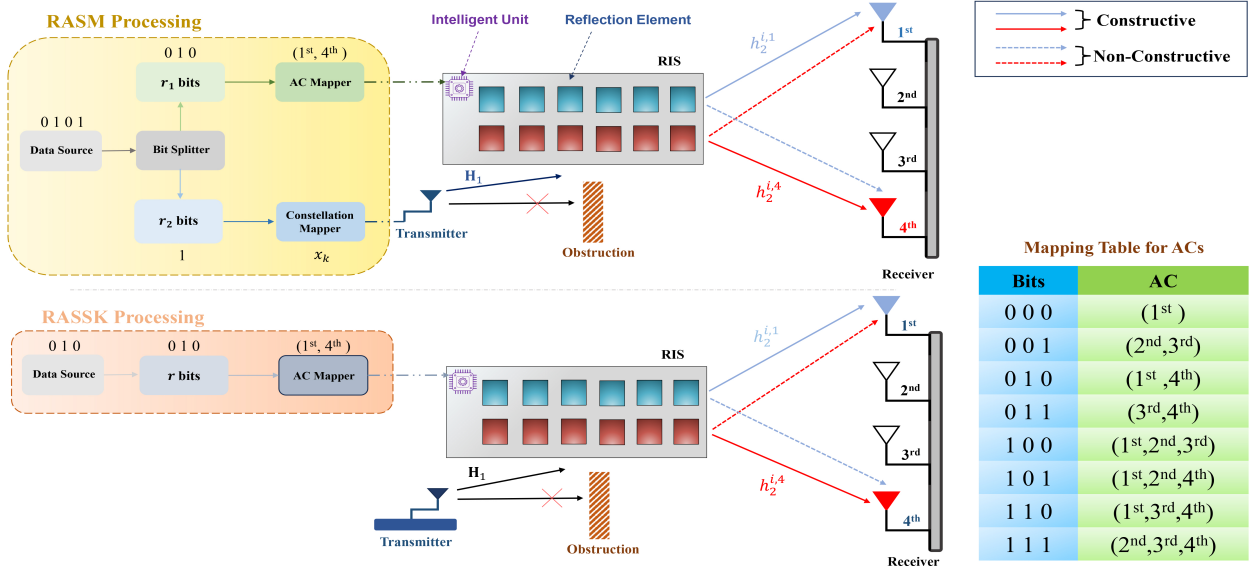


Fig. 1. System models for the RASM and RASSK schemes.

approach enables straightforward implementation at intelligent unit, which parses the bit sequence to identify the AC and sorts indices before phase adjustment. **It ensures fairness by allocating equal RE resources to each selected AC, strictly avoiding the overhead associated with real-time dynamic channel optimization algorithms, ensuring high efficiency.**

5) *Rician Channel Fading*: To better model a practical wireless environment for the proposed schemes, the Rician channel fading can also be taken into account. This type of fading is appropriate when there is a strong line-of-sight (LoS) path between the RIS and the receiver. The Rician distribution of $h_2^{i,n}$ can be given as

$$h_2^{i,n} = \sqrt{\frac{K}{K+1}} h_{2,Los}^{i,n} + \sqrt{\frac{1}{K+1}} h_{2,NLos}^{i,n}, \quad (1)$$

where $h_{2,Los}^{i,n}$ represents the deterministic LoS component and $h_{2,NLos}^{i,n}$ is a zero-mean complex Gaussian random variable accounting for the non-LoS multi-path components. The Rician factor $K \geq 0$ denotes the ratio of the power in the LoS component to that in the scattered components. When $K = 0$, the model reduces to Rayleigh fading, while higher K values indicate a stronger LoS presence.

B. RASM Transmission

Assuming total b_{RASM} bits are required to transmit, b_{RASM} bits can be divided into b_1 and b_2 bits in the RASM scheme, where b_1 bits are mapped into the indices of selected antenna combinations at receiver and b_2 bits are mapped into the ones mapping to M -ary PSK/QAM symbol transmitted from the transmitter, as shown in Fig. 1. For the selected AC, each one represents different bit sequence, e.g., the third selected AC indicates the bits 010. Moreover, the last bit in sequence is 1, which is represented by k -th constellation symbol x_k in M -ary PSK/QAM constellation symbol vector as $\mathbf{x}_k = [x_1, x_2, \dots, x_M]^T$ as shown in Fig. 1. The expression for the

received signal in the RASM scheme can be written as

$$\mathbf{Y} = \mathbf{H}_2 \Phi_r \mathbf{H}_1 x_k + \mathbf{N}, \quad (2)$$

where $\Phi_r \in \mathbb{C}^{N \times N}$ represents the diagonal matrix of adjusted phase for r -th AC is the vector of Gaussian white noise. However, to better show the differences between various indices of ACs, we give the received signal expression at l -th receive antenna in r -th selected AC without Gaussian white noise τ_l , which is expressed as

$$y_l' = \underbrace{\sum_{i=(l-1)N_E+1}^{N_E} h_2^{i,l} \Phi_{i,l} h_1^i x_k}_{\text{constructive part}} + \underbrace{\sum_{q=1, q \neq l}^{N_a} \sum_{i=i'}^{qN_E} h_2^{i,l} \Phi_{i,l} h_1^i x_k}_{\text{non-constructive part}}, \quad (3)$$

with $i' = (q-1)N_E + 1$, as extended as ³

$$y_l' = \underbrace{\sum_{q=1, q \neq z}^{N_a} \sum_{i=i'}^{qN_E} \beta_{i,l} \alpha_i e^{j\Psi_{i,l}} x_k}_{\text{non-constructive part}} + \underbrace{\sum_{i=(l-1)N_E+1}^{lN_E} \beta_{i,l} \alpha_i x_k}_{\text{constructive part}}, \quad (4)$$

where $\Phi_{i,l}$ can be simplified as $\exp(j\Psi_{i,l})$ representing the adjust phase of the i -th RE and for the l -th selected receive antenna in selected AC, $\Psi_{i,l} = \varphi_i - \omega_{i,l} - \theta_i$, $l \in \{1, \dots, N_a\}$. In the meanwhile, the complete received signal at l -th selected antenna is given as $y_l = y_l' + \tau_l$ with τ_l representing the Gaussian white noise at l -th selected receive antenna in selected AC with $\mathcal{CN}(0, N_0)$ distribution. In Eq. (3) and (4), note that regarding the beam from non-constructive parts and beam narrowness in dense arrays, e.g., $\frac{\lambda}{2}$ spacing, the model incorporates non-constructive reflections, i.e., side lobes and interference, avoiding the assumption of zero interference. And

³We assume that each part of REs can perfectly achieve the passive beamforming for specific l -th selected antenna as $\varphi_i = \omega_{i,l} + \theta_i$ [13]-[16].

the received signal of u -th unselected received antenna can be given as

$$y_u = \sum_{q=1}^{N_a} \sum_{i=(q-1)N_E+1}^{qN_E} \beta_{i,u} \alpha_i e^{j(\varphi_i - \omega_{i,l} - \theta_i)} x_k + \tau_u, \quad (5)$$

with which the SNR can be obtained as

$$\gamma_u = \frac{\left\| \sum_{q=1}^{N_a} \sum_{i=(q-1)N_E+1}^{qN_E} \beta_{i,u} \alpha_i e^{j(\varphi_i - \omega_{i,l} - \theta_i)} x_k \right\|^2}{N_0}. \quad (6)$$

According to the characteristic of the RIS, when $\varphi_i = \omega_{i,l} + \theta_i$, the SNR at l -th selected antenna can be maximized, which is given as

$$\begin{aligned} \{\gamma_l\}_{max} &= \frac{\left| \sum_{i=(l-1)N_E+1}^{lN_E} \beta_{i,l} \alpha_i x_k \right|^2}{N_0} \\ &+ \frac{\left| \sum_{q=1, q \neq l}^{N_a} \sum_{i=(q-1)N_E+1}^{qN_E} \beta_{i,l} \alpha_i e^{j(\varphi_i - \omega_{i,l} - \theta_i)} x_k \right|^2}{N_0}. \end{aligned} \quad (7)$$

Applying the ML detector, the expression of ML detection in the RASM scheme can be given as follows:

$$\{\hat{r}, \hat{k}\} = \arg \min_{r,k} \|\mathbf{Y} - \mathbf{G}_{r,k}\|_2^2, \quad (8)$$

where \hat{r} and \hat{k} represent the estimated r -th AC and k -th M -ary PSK/QAM symbol, and $\mathbf{G}_{r,k} = \mathbf{H}_2 \Phi_r \mathbf{H}_1 x_k$. Here, $\mathbf{G}_{r,k}$ can be rewritten as $\mathbf{G}_{r,k} = \{G_n\}_{n=1}^{N_r}$, where G_n is

$$G_n = \begin{cases} \sum_{i=(l-1)N_E+1}^{lN_E} h_2^{i,n} h_1^i x_k + G'_n, & v_{r,n} = 1 \\ \sum_{q=1}^{N_a} \sum_{i=(q-1)N_E+1}^{qN_E} \beta_{i,u} \alpha_i e^{j\psi_{i,l}} x_k, & v_{r,n} = 0 \end{cases} \quad (9)$$

with $G'_n = \sum_{q=1, q \neq l}^{N_a} \sum_{i=c}^{qN_E} h_2^{i,n} \Phi_{i,l} h_1^i x_k$.

C. RASSK Transmission

In the RASSK scheme, b_{RASSK} bits are transmitted to the receiver, which are all mapped into the indices of ACs by the receiver. Similar to the above steps, the received signal expression of the RASSK scheme without the constellation symbols can be given as

$$\mathbf{Y} = E_s \mathbf{H}_2 \Phi_r \mathbf{H}_1 + \mathbf{N}, \quad (10)$$

where E_s represents the transmitted energy. The received signal expression without Gaussian white noise at l -th receive antenna for the selected AC in the RASSK scheme is

$$\begin{aligned} y'_l &= E_s \underbrace{\sum_{i=(l-1)N_E+1}^{N_E} \beta_{i,l} \alpha_i}_{\text{constructive part}} \\ &+ \underbrace{E_s \sum_{q=1, q \neq l}^{N_a} \sum_{i=(q-1)N_E+1}^{qN_E} \beta_{i,l} \alpha_i e^{j\psi_{i,l}}}_{\text{non-constructive part}}, \end{aligned} \quad (11)$$

which, including Gaussian white noise, can be expressed as τ_l as $y_l = y'_l + \tau_l$. In the meanwhile, the received signal of u -th

unselected received antenna in the RASSK scheme is

$$\begin{aligned} y_u &= E_s \sum_{q=1}^{N_a} \sum_{i=(q-1)N_E+1}^{qN_E} h_2^{i,u} \Phi_{i,l} h_1^i + \tau_u \\ &= E_s \sum_{q=1}^{N_a} \sum_{i=(q-1)N_E+1}^{qN_E} \beta_{i,u} \alpha_i e^{j(\varphi_i - \omega_{i,l} - \theta_i)} + \tau_u. \end{aligned} \quad (12)$$

Thus, the received SNR at u -th unselected antenna is:

$$\gamma_u = \frac{E_s \left\| \sum_{q=1}^{N_a} \sum_{i=(q-1)N_E+1}^{qN_E} \beta_{i,u} \alpha_i e^{j(\varphi_i - \omega_{i,l} - \theta_i)} \right\|^2}{N_0}, \quad (13)$$

and then it can be maximized through $\varphi_i = \omega_{i,u} + \theta_i$ at l -th selected antenna can be given as

$$\begin{aligned} \{\gamma_l\}_{max} &= E_s \frac{\left| \sum_{i=(l-1)N_E+1}^{lN_E} \beta_{i,l} \alpha_i \right|^2}{N_0} \\ &+ E_s \frac{\left| \sum_{q=1, q \neq l}^{N_a} \sum_{i=(q-1)N_E+1}^{qN_E} \beta_{i,l} \alpha_i e^{j\psi_{i,l}} \right|^2}{N_0}. \end{aligned} \quad (14)$$

The ML detector of the RASSK scheme can be given a

$$\{\hat{r}\} = \arg \min_r \|\mathbf{Y} - \mathbf{G}_r\|_2^2 \quad (15)$$

with $\mathbf{G}_r = E_s \mathbf{H}_2 \Phi_r \mathbf{H}_1$. Meanwhile, \mathbf{G}_r can be rewritten as $\mathbf{G}_r = \{G_n\}_{n=1}^{N_r}$, where G_n can be expressed as

$$G_n = \begin{cases} E_s \left\{ \sum_{i=(l-1)N_E+1}^{lN_E} h_2^{i,n} h_1^i + G'_n \right\}, & v_{r,n} = 1 \\ E_s \left\{ \sum_{q=1}^{N_a} \sum_{i=(q-1)N_E+1}^{qN_E} \beta_{i,u} \alpha_i e^{j\psi_{i,l}} \right\}, & v_{r,n} = 0 \end{cases} \quad (16)$$

with $G'_n = E_s \sum_{q=1, q \neq l}^{N_a} \sum_{i=c}^{qN_E} h_2^{i,n} \Phi_{i,l} h_1^i$. Similar to example of RASM in Fig. 1, transmitted bit sequence 010 is mapped into 1st and 4th receive antennas, then successfully being detected at receiver.

D. Impact of Quantized RIS Phase Errors

In practical deployments, achieving perfect continuous phase shifts is highly challenging due to hardware impairments and the limited resolution of phase shifters, i.e., finite discrete phase quantization. To account for these practical hardware limitations, a phase error term $\Delta\varphi_{i,m}$ can be introduced. The ideal adjusted phase matrix Φ_r is replaced by the practical phase matrix with errors, denoted as $\tilde{\Phi}_r$, which is given as

$$\tilde{\Phi}_r = \text{diag} \left(e^{j(\varphi_{1,m} + \Delta\varphi_{1,m})}, \dots, e^{j(\varphi_{N,m} + \Delta\varphi_{N,m})} \right), \quad (17)$$

with $\Delta\varphi_{i,m}$ representing the phase error of the i -th reflecting element intended for the m -th receive antenna. For a b -bit quantized RIS, this phase error is typically modeled as an independent uniform random variable distributed over $[-\frac{\pi}{2^b}, \frac{\pi}{2^b}]$. Consequently, the received signal expressions for the RASM and RASSK schemes, originally given in Eq. (2) and Eq. (10), respectively, must be modified to incorporate these hardware

impairments:

$$\tilde{\mathbf{Y}}_{\text{RASM}} = \mathbf{H}_2 \tilde{\Phi}_r \mathbf{H}_1 x_k + \mathbf{N}, \quad (18)$$

$$\tilde{\mathbf{Y}}_{\text{RASSK}} = E_s \mathbf{H}_2 \tilde{\Phi}_r \mathbf{H}_1 + \mathbf{N}. \quad (19)$$

Due to the presence of the phase error $\Delta\varphi_{i,m}$, the perfect passive beamforming condition ,e.g., $\varphi_i = \omega_{i,l} + \theta_i$, required to maximize the SNR cannot be strictly satisfied.⁴

III. GENERALIZED PRE-DEFINED ACS SELECTION

Due to the obstruction of the direct link from the RIS to the transmitter and phase adjustment is only optimized for the receiver, obtaining perfect instantaneous CSI from the receiver to the RIS and from the RIS to the transmitter is extremely challenging at the transmitter. Meanwhile, estimating instantaneous CSI for each time slot is not high-efficient due to its high computational complexity and additional spectrum resource requirements, which are especially not practical in future wireless networks.

Since the total number of mathematically available ACs is $J = 2^{N_r} - 1$, but the number of required ACs for bit mapping must be a power of 2, the available ACs are typically more than required. For instance, 3 receive antennas yield 7 non-empty ACs, but only 4 are required to represent 2 bits. Therefore, a generalized pre-defined ACs selection algorithm is essential to eliminate the unnecessary ACs. Before transmission, the transmitter and the receiver pre-agree that exactly D ACs will be utilized to convey the $b_1 = \lfloor \log_2(2^{N_r} - 1) \rfloor$ bits, where $D = 2^{b_1}$. These D ACs are chosen from the set of non-empty receive subsets through a specific sequence. In our proposed scheme, we first systematically eliminate the ACs containing the maximum number of antennas, i.e., $N_a = N_r$. Subsequently, we sort the remaining ACs in ascending order based on their N_a . Finally, the first D ACs in this sorted list are selected for bit mapping. By employing this method, we not only exclude the ACs with the maximum N_a but also minimize the involvement of ACs with higher N_a in subsequent signal processing stages, which effectively mitigates the impacts of the non-constructive interference. As a concrete example, assuming $N_r = 4$, we need to select $D = 2^3 = 8$ ACs from the 15 available ones. By following the aforementioned steps, the single AC with $N_a = 4$ and a majority of the ACs with $N_a = 3$ are systematically eliminated. The final selected AC set is denoted as $\Lambda(r)$ with $r = 1, 2, \dots, D$. This designed selection significantly reduces the detection complexity, as detailed in Sec. IV.C. The designed selection can significantly reduce the detection complexity, and a detailed analysis of its detection complexity is provided in sub-section B of Sec. IV. The generalized pre-defined ACs selection works at the intelligent unit of the RIS after the information of selected ACs inputting. Then, the intelligent unit controls various parts of REs to amplify the transmitted signal for the specific receive antenna/antennas. **By intelligently pruning the transmission**

⁴While this foundational work evaluates the proposed schemes under imperfect CSI and Rician fading, practical deployments face additional impairments like CSI feedback delays, hardware non-idealities, and frequency-selective fading. Incorporating these dynamic factors would render the closed-form analysis mathematically intractable. Therefore, a comprehensive investigation of these practical impairments is left for future research.

states rather than relying solely on post-processing at the receiver, this mechanism intrinsically resolves the complexity bottleneck of dynamic RIS beamforming.

IV. PERFORMANCE ANALYSIS

In this section, we discuss the performance analysis of the RASM and RASSK schemes in terms of SE, BER, and detection complexity. Firstly, the SE performance of the proposed schemes is presented. Notably, to better demonstrate and understand the SE performance, we utilize the bit per channel use (bpcu) of various IM schemes to represent and discuss the SE performance. Secondly, we derive and analyze the upper bound of the average BER (ABER) to represent the BER performance of both proposed schemes, assuming Rayleigh channel fading and the use of the ML detector. Furthermore, the complexity of ML detector in the proposed schemes and other related schemes is discussed.

A. SE Performance

For each time slot, in the RASM scheme, the SE of b_1 bits mapped into ACs can be expressed as

$$SE_1 = \lfloor \log_2 J \rfloor = \lfloor \log_2 (2^{N_r} - 1) \rfloor, \quad (20)$$

and the SE of b_2 bits mapped into constellation symbols can be given as $SE_2 = \log_2 M$. Thus, the total SE of the RASM can be obtained by $SE_1 + SE_2$ as

$$SE_{\text{RASM}} = \lfloor \log_2 (2^{N_r} - 1) \rfloor + \log_2 M. \quad (21)$$

Meanwhile, the SE of the RASSK scheme can be given as

$$SE_{\text{RASSK}} = \lfloor \log_2 (2^{N_r} - 1) \rfloor. \quad (22)$$

In order to show the superiority in the SE of the RASM and RASSK schemes, we also provide the SE expression of the RSM, RSSK schemes, which are given respectively as follows:

$$SE_{\text{RSM}} = \log_2 N_r + \log_2 M, \quad (23)$$

$$SE_{\text{RSSK}} = \log_2 N_r. \quad (24)$$

Furthermore, the RGSM and RGSSK schemes, as the schemes with higher SE than that of the RSM and RSSK schemes, have a fixed number of selected antennas as N_s in each time slot to convey signals, of which the SE can be given as

$$SE_{\text{RGSM}} = \left\lfloor \log_2 \left(\frac{N_s}{N_r} \right) \right\rfloor + \log_2 M, \quad (25)$$

$$SE_{\text{RGSSK}} = \left\lfloor \log_2 \left(\frac{N_s}{N_r} \right) \right\rfloor. \quad (26)$$

Remark 1: Comparing Eq. (21) and Eq. (22), we can easily find that $SE_{\text{RASM}} > SE_{\text{RASSK}}$ with the same N_r , and the SE of both schemes increases with the increase of N_r . In order to conduct more impartial SE comparisons, by comparing Eq. (21), Eq. (23), Eq. (25) and Eq. (22), Eq. (24), Eq. (26) respectively, we can draw an insightful conclusion as $SE_{\text{RASM}} \geq SE_{\text{RGSM}} > SE_{\text{RSM}}$ and $SE_{\text{RASSK}} \geq SE_{\text{RGSSK}} > SE_{\text{RSSK}}$ with same N_r and M , where the equivalence sign can be applicable when N_r is large enough and $N_s > 2$. However, the BER performance of the RGSM and RGSSK

schemes has significant deterioration when $N_s > 2$, but the RASM and RASSK schemes still exhibit better performance while remaining the same N_r .

B. BER Performance

This subsection provides the analytical performance in ABER of both RASM and RASSK schemes, where some insights are also given with $x_k = x_{\hat{k}} = \sqrt{E_s}$ and Rician channel fading with $K = 0$ is considered.

1) *ABER for the RASM Scheme*: The analytical ABER of the RASM scheme is given. According to Eq. (8) of ML detector, the instantaneous pairwise error probability (PEP) can be expressed by giving channel h_1^i and $h_2^{i,l}$ as

$$\begin{aligned} \Pr(\{r, k\} \rightarrow \{\hat{r}, \hat{k}\} | h_1^i, h_2^{i,m}) &= \Pr(\|\mathbf{Y} - \mathbf{G}_{r,k}\|_2^2) \\ &= \Pr\left(\sum_{n=1}^{N_r} \|y_n - G_n\|_2^2 > \sum_{n=1}^{N_r} \|y_n - \hat{G}_n\|_2^2\right), \end{aligned} \quad (27)$$

where \hat{G}_n represents the estimated G_n and y_n represents the received signal at n -th receive antenna. After some algebraic operations, Eq. (27) can be extended and rewritten as

$$\Pr(\{r, k\} \rightarrow \{\hat{r}, \hat{k}\} | h_1^i, h_2^{i,m}) = \Pr(\Gamma < 0), \quad (28)$$

with

$$\Gamma = \sum_{n=1}^{N_r} \|G_n - \hat{G}_n\|_2^2 + \sum_{n=1}^{N_r} 2\Re\{\tau_n^* [G_n - \hat{G}_n]\}, \quad (29)$$

where τ_n^* represents the complex conjugation of Gaussian white noise and $\Gamma \sim \mathcal{N}(\mu_\Gamma, \sigma_\Gamma^2)$ with $Z = \sum_{n=1}^{N_r} \|G_n - \hat{G}_n\|_2^2$ and $\sigma_\Gamma^2 = 2N_0 \sum_{n=1}^{N_r} \|G_n - \hat{G}_n\|_2^2$. Thus, by applying the Gaussian Q-function as $Q(\frac{-\mu_\Gamma}{\sigma_\Gamma})$ the PEP can be further denoted as follows:

$$\Pr(\{r, k\} \rightarrow \{\hat{r}, \hat{k}\} | h_1^i, h_2^{i,m}) = Q\left(\sqrt{\frac{Z}{2N_0}}\right). \quad (30)$$

Considering the alternative form of Q-function, the unconditional PEP, which is averaged over channel coefficients as $\Pr(\{r, k\} \rightarrow \{\hat{r}, \hat{k}\}) = \mathbb{E}_Z\left[Q\left(\sqrt{\frac{Z}{2N_0}}\right)\right]$, is calculated as

$$\begin{aligned} \Pr(\{r, k\} \rightarrow \{\hat{r}, \hat{k}\}) &= \int_0^\infty Q\left(\sqrt{\frac{Z}{2N_0}}\right) f_Z(Z) dZ \\ &= \frac{1}{\pi} \int_0^{\frac{\pi}{2}} M_Z\left(\frac{-1}{4\sin^2 \tau N_0}\right) d\tau, \end{aligned} \quad (31)$$

which applies the moment generating function (MGF) of Z , given as $M_Z(t) = \int_0^\infty e^{tZ} dZ$, with $t = \frac{-1}{4\sin^2 \tau N_0}$. Actually, Z is the squared Euclidean distance (SED) between the symbols $G_{r,k}$ and $G_{\hat{r},\hat{k}}$. Here, the MGF of Eq. (31) is derived by the general quadratic form of correlated Gaussian random variables and counts on erroneous or correct detection of the r -th and \hat{r} -th AC indices. Note that the error in the detection of AC index is able to affect the accuracy of constellation symbol detection. Thus, we separate Z into two categories, which are given as: $Z_1 = \{Z | r \neq \hat{r}\}$ and $Z_2 = \{Z | r = \hat{r}\}$. 1) First case $Z_1: \{Z | r \neq \hat{r}\}$

In this case, the SED can be given as $Z_1 = Z_1^1 + Z_1^2 + Z_1^3$, which are given specifically in Eq. (32), Eq. (33), and Eq. (34) with $\varphi_i - \omega_{i,l} - \theta_i = \Psi_{i,l}$, as shown at the top of next page.

Here, Z_1^1 , Z_1^2 , and Z_1^3 stand for the $m = r$, $m = \hat{r}$, and $m \neq r, \hat{r}$ respectively. Then, we can denote Z_1^1 and Z_1^2 as

$$Z_1^1 = |q_1|^2 = (q_1)_{\Re}^2 + (q_1)_{\Im}^2, \quad (35)$$

$$Z_1^2 = |q_2|^2 = (q_2)_{\Re}^2 + (q_2)_{\Im}^2, \quad (36)$$

where q_1 and q_2 follow complex Gaussian distribution by applying central limit theorem (CLT).^{5 6} The mean vector $\boldsymbol{\mu}_1$ and covariance matrix $\boldsymbol{\sigma}_1^2$ of $\mathbf{z}_1 = [(q_1)_{\Re}, (q_1)_{\Im}, (q_2)_{\Re}, (q_2)_{\Im}]$, which are respectively given:

$$\boldsymbol{\mu}_1 = \frac{N\pi}{4} [(x_k)_{\Re}, (x_k)_{\Im}, -(x_k)_{\Re}, -(x_k)_{\Im}]^T, \quad (37)$$

$$\boldsymbol{\sigma}_1^2 = \begin{bmatrix} \sigma_{1,1}^2 & \sigma_{1,2}^2 & \sigma_{1,3}^2 & \sigma_{1,4}^2 \\ \sigma_{1,2}^2 & \sigma_{2,2}^2 & \sigma_{2,3}^2 & \sigma_{2,4}^2 \\ \sigma_{1,3}^2 & \sigma_{2,3}^2 & \sigma_3^2 & \sigma_{3,4}^2 \\ \sigma_{1,4}^2 & \sigma_{2,4}^2 & \sigma_{3,4}^2 & \sigma_4^2 \end{bmatrix}, \quad (38)$$

where

$$\begin{aligned} \sigma_1^2 &= N_a \left[\left(N_a - \frac{\pi^2}{16}\right) N_E (x_k)_{\Re}^2 + \frac{N |x_k|^2}{2} \right], \\ \sigma_2^2 &= N_a \left[\left(N_a - \frac{\pi^2}{16}\right) N_E (x_k)_{\Im}^2 + \frac{N |x_k|^2}{2} \right], \\ \sigma_3^2 &= N_a \left[\left(N_a - \frac{\pi^2}{16}\right) N_E (x_k)_{\Re}^2 + \frac{N |x_k|^2}{2} \right], \\ \sigma_4^2 &= N_a \left[\left(N_a - \frac{\pi^2}{16}\right) N_E (x_k)_{\Im}^2 + \frac{N |x_k|^2}{2} \right]. \end{aligned} \quad (39)$$

By applying the property of covariance between two random variables X and Y as

$$2\text{Cov}(X, Y) = \mathbb{D}[X + Y] - \mathbb{D}[X] - \mathbb{D}[Y], \quad (40)$$

we can easily obtain the $\sigma_{1,2}^2$, $\sigma_{3,4}^2$, $\sigma_{1,4}^2$, $\sigma_{2,3}^2$, and $\sigma_{2,4}^2$. The MGF of the generalized non-central chi-square distribution is

⁵Note that α and β are the magnitudes of standard complex Gaussian random variables, they follow the Rayleigh distribution with mean value $\frac{\sqrt{\pi}}{2}$ variance $\frac{4-\pi}{4}$, respectively. Moreover, since ω_i , φ_i , and θ_i are the phase of standard complex Gaussian random variable and follow the uniform distribution at the range in $(-\pi, \pi)$.

⁶It should be noted that the derived ABER expressions rely on the CLT approximation, which is asymptotically accurate. In practical RIS-assisted systems, the reliability of this approximation depends on the number of reflecting elements L_i assigned to each receive antenna. Through numerical validation, we observe that the approximation remains highly precise when $L_i \geq 8$. As L_i or the total RIS size N increases, the aggregate channel distribution further converges to the complex Gaussian model, making the analytical results more precise.

$$Z_1^1 = \sum_{l \in V_r} \left| \left(\sum_{i=(l-1)N_E+1}^{lN_E} \beta_{i,l} \alpha_i + \sum_{q=1, q \neq l}^{N_a} \sum_{i=(q-1)N_E+1}^{qN_E} \beta_{i,l} \alpha_i e^{j\psi_{i,l}} \right) x_k - \sum_{q=1}^{N_a} \sum_{i=(q-1)N_E+1}^{qN_E} \beta_{i,l} \alpha_i e^{j\psi_{i,l}} x_{\hat{k}} \right|^2, \quad (32)$$

$$Z_1^2 = \sum_{\hat{l} \in V_{\hat{r}}} \left| \sum_{q=1}^{N_a} \sum_{i=(q-1)N_E+1}^{qN_E} \beta_{i,\hat{l}} \alpha_i e^{j\psi_{i,\hat{l}}} x_k - \left(\sum_{i=(l-1)N_E+1}^{lN_E} \beta_{i,\hat{l}} \alpha_i + \sum_{q=1, q \neq l}^{N_a} \sum_{i=(q-1)N_E+1}^{qN_E} \beta_{i,\hat{l}} \alpha_i e^{j\psi_{i,\hat{l}}} \right) x_{\hat{k}} \right|^2, \quad (33)$$

$$Z_1^3 = \sum_{n=1, n \neq l, n \neq \hat{l}}^{N_r} \left| \sum_{q=1}^{N_a} \sum_{i=(q-1)N_E+1}^{qN_E} \left(\beta_{i,n} \alpha_i e^{j(\varphi_i - \omega_{i,l} - \theta_i)} x_k - \beta_{i,n} \alpha_i e^{j(\varphi_i - \omega_{i,l} - \theta_i)} x_{\hat{k}} \right) \right|^2. \quad (34)$$

given as follows [15]-[16]:

$$M_X(t | \boldsymbol{\mu}, \boldsymbol{\sigma}^2) = [\det(\mathbf{E} - 2t\boldsymbol{\sigma}^2)]^{-\frac{1}{2}} \times \exp \left\{ -\frac{1}{2} \boldsymbol{\mu}^T [\mathbf{E} - (\mathbf{E} - 2t\boldsymbol{\sigma}^2)^{-1}] \boldsymbol{\sigma}^{-1} \boldsymbol{\mu} \right\}, \quad (41)$$

where $X = \sum_{f=1}^f X_f^2$, is the unit matrix, $\boldsymbol{\mu}$ and $\boldsymbol{\sigma}^2$ represent the mean vector and covariance matrix of $[X_1, X_2, \dots, X_f]^T$. Then, substituting Eq. (37) and Eq. (38) into Eq. (41), we can yield the MGF of $Z_1^1 + Z_1^2$, given as $M_{Z_1^1+Z_1^2}(t | \boldsymbol{\mu}_1, \boldsymbol{\sigma}_1^2)$. Nevertheless, the MGF of Z_1^3 is still needed to be derived. In Eq. (34), we define that

$$\Gamma = \sum_{q=1}^{N_a} \sum_{i=(q-1)N_E+1}^{qN_E} \beta_{i,n} \alpha_i e^{j(\varphi_i - \omega_{i,l} - \theta_i)} x_k - \sum_{q=1}^{N_a} \sum_{i=(q-1)N_E+1}^{qN_E} \beta_{i,n} \alpha_i e^{j(\varphi_i - \omega_{i,l} - \theta_i)} x_{\hat{k}}, \quad (42)$$

which has variance $\sigma_\Gamma^2 = \frac{N(|x_k|^2 + |x_{\hat{k}}|^2)}{2}$ and zero mean value. For Eq. (34), Z_1^3 follows the generalized central chi-square distribution with $2(D-2)N_a$ degree of freedom and has MGF:

$$M_{Z_1^3}(t) = \left[1 - tN \left(|x_k|^2 + |x_{\hat{k}}|^2 \right) \right]^{-\frac{N_l}{2}}, \quad (43)$$

where N_l represents the number of same antennas in the selected AC and estimated AC. Finally, the MGF of Z_1 can be obtained as

$$M_{Z_1}(t) = M_{Z_1^1+Z_1^2}(t | \boldsymbol{\mu}_1, \boldsymbol{\sigma}_1^2) M_{Z_1^3}(t). \quad (44)$$

And the unconditional PEP of case 1 can be given by substituting Eq. (44) into Eq. (31) as

$$\begin{aligned} P_{rZ_1}(\{r, k\} \rightarrow \{\hat{r}, \hat{k}\}) \\ = \frac{1}{\pi} \int_0^{\frac{\pi}{2}} M_{Z_1^1+Z_1^2}(t | \boldsymbol{\mu}_1, \boldsymbol{\sigma}_1^2) M_{Z_1^3}(t) d\tau. \end{aligned} \quad (45)$$

2) Second case $Z_2: \{Z | r = \hat{r}\}$:

In this case, we also can divide Z_2 into $Z_2^1 + Z_2^2$ with

$$Z_2^1 = |x_k - x_{\hat{k}}|^2 \sum_{l \in V} \left| \sum_{q=1, q \neq l}^{N_a} \sum_{i=(q-1)N_E+1}^{qN_E} \beta_{i,l} \alpha_i e^{j\psi_{i,l}} \right|^2 + |x_k - x_{\hat{k}}|^2 \sum_{l \in V_r} \left| \sum_{i=(l-1)N_E+1}^{N_E} \beta_{i,l} \alpha_i \right|^2, \quad (46)$$

$$Z_2^2 = |x_k - x_{\hat{k}}|^2 \sum_{n=1, n \neq l}^{N_r} \left| \sum_{q=1}^{N_a} \sum_{i=i'}^{qN_E} \beta_{i,n} \alpha_i e^{j(\varphi_i - \omega_{i,l} - \theta_i)} \right|^2, \quad (47)$$

where Z_2^1 and Z_2^2 stand for the situations that $m = r$ and $m \neq r$, respectively. Firstly, by approximating $\beta_{i,l} \alpha_i$ as a Gaussian random variable with CLT, the mean value and variance of Z_2^1 can be obtained as $\mu_{Z_2^1} = \frac{N_a N_E \pi |x_k - x_{\hat{k}}|}{4}$ and $\sigma_{Z_2^1}^2 = \frac{|x_k - x_{\hat{k}}|^2 N_a N_E (32 - \pi^2)}{16}$. Then, by substituting $\mu_{Z_2^1}$ and $\sigma_{Z_2^1}^2$ into Eq. (41), the MGF of Z_2^1 can be obtained as

$$M_{Z_2^1}(t | \mu_{Z_2^1}, \sigma_{Z_2^1}^2) = \left(1 - 2\sigma_{Z_2^1}^2 t \right)^{-\frac{1}{2}} e^{-\frac{t \mu_{Z_2^1}^2}{1 - 2\sigma_{Z_2^1}^2 t}}. \quad (48)$$

Secondly, Γ_2 can be approximately considered as a Gaussian random variable applying CLT:

$$\Gamma_2 = \sum_{q=1}^{N_a} \sum_{i=(q-1)N_E+1}^{qN_E} \beta_{i,n} \alpha_i e^{j\psi_{i,l}} x_k, \quad (49)$$

with zero mean value and variance $\sigma_{\Gamma_2}^2 = N$. Thus, Z_2^2 follows the generalized non-central chi-square distribution with $(N_r - N_a)$ degree of freedom and has the variance denoted as $\sigma_{Z_2^2}^2 = \frac{N N_a |x_k - x_{\hat{k}}|^2}{2}$. Giving $\sigma_{Z_2^2}^2$ and following Eq. (44), the MGF of Z_2^2 yields as

$$M_{Z_2^2}(t) = \left(1 - t N_a N |x_k - x_{\hat{k}}|^2 \right)^{-\frac{N_r - N_a}{2}}. \quad (50)$$

Thus, the MGF of Z_2 can be obtained by multiplying Eq. (48) and Eq. (50), which is specifically given as $M_{Z_2}(t) = M_{Z_2^1}(t) M_{Z_2^2}(t)$, which can be substituted into Eq. (31) to

further obtain the unconditional PEP of case 2⁷ as

$$P_{rZ_2} \left(\{r, k\} \rightarrow \{\hat{r}, \hat{k}\} \right) = \frac{1}{\pi} \int_0^{\frac{\pi}{2}} M_{Z_2}(t) d\tau. \quad (51)$$

Eventually, the union bound of ABER for the RASM scheme can be derived from the values of unconditional PEP by Eq. (27), which is given as

$$P_b^{RASM} \leq \frac{\sum_r \sum_{\hat{r}} \sum_k \sum_{\hat{k}} P_r \left(\{r, k\} \rightarrow \{\hat{r}, \hat{k}\} \right) e'}{MD \log_2(MD)}, \quad (52)$$

where $e' = e \left(\{r, k\} \rightarrow \{\hat{r}, \hat{k}\} \right)$ represents the number of bits in error for the corresponding pairwise error event. Based on this analytical ABER, more insights of the BER performance can be found with the simulation results in Sec. IV.

2) *ABER for the RASSK Scheme*: The analytical ABER performance of the RASSK scheme with the ML detector is given in this sub-section. In light of the steps in ABER derivations of the RASM scheme with the ML detector, the conditional PEP of it can be given:

$$P_r \left(r \rightarrow \hat{r} \mid h_1^i, h_2^{i,m} \right) \stackrel{\text{def}}{=} Q \left(\sqrt{\frac{B}{2N_0}} \right), \quad (53)$$

where $B = \sum_{n=1}^{N_r} \|G_n - G_{\hat{n}}\|_2^2$. Then, by averaging over channel coefficients, the average unconditional PEP can be obtained as

$$P_r(r \rightarrow \hat{r}) = \frac{1}{\pi} \int_0^{\frac{\pi}{2}} M_B \left(\frac{-1}{4 \sin^2 \tau N_0} \right) d\tau. \quad (54)$$

Since the constellation symbols are not transmitted in the RASSK scheme and $x_k = x_{\hat{k}} = \sqrt{E_s}$, case 1 in the ABER analysis of the RASM scheme with the ML detector is also suitable for the RASSK one where $r \neq \hat{r}$. In other words, the MGF given in Eq. (41) of the RASM scheme in case 1 can be also employed in the RASSK scheme with some modifications in x_k and E_s , i.e., $M_B \left(\frac{-1}{4 \sin^2 \tau N_0} \right) \approx M_{Z_1}(t)$. Finally, the upper bound of the RASSK scheme with the ML detector can be obtained similar to

$$P_b^{RASSK} \leq \frac{\sum_r \sum_{\hat{r}} P_r(r \rightarrow \hat{r}) e(r \rightarrow \hat{r})}{D \log_2(D)}. \quad (55)$$

Remark 2: Since the increase of N leads to the increase of N_E and probably N_a , we can find that the results of above MGFs decrease with the arise of N , which means that the ABER reduces with the N increase.

Remark 3: **The theoretical rigor of this framework is established as follows: First, the ABER expressions in Eq. (52) and Eq. (55) provide strict theoretical upper bounds derived via the MGF approach. Second, the deterministic even division strategy for RIS phase adjustment circumvents the need for algorithmic convergence proofs, while the ML detector ensures detection optimality. Although employing the CLT for mathematical tractability, the tightness of this asymptotic analysis**

⁷Following the upper bound of Q-function, the PEP can be expressed as $P_r \left(\{r, k\} \rightarrow \{\hat{r}, \hat{k}\} \right) \leq \frac{1}{6} M_Z \left(-\frac{1}{N_0} \right) + \frac{1}{12} M_Z \left(-\frac{1}{2N_0} \right) + \frac{1}{4} M_Z \left(-\frac{1}{4N_0} \right)$ [29]. The closed-form expression can be obtained in this way, which is not extended in this paper.

is robustly validated by Monte Carlo simulations in Sec. VI.

C. Detection Complexity

In this section, the complexity of the ML detector in the RASM and RASSK schemes are analyzed. We calculate the complexity based on Eq. (8) in the RASM scheme and Eq. (15) in the RASSK scheme, where the complex multiplications (CM) and complex additions (CA) are all required to count [30]-[32]. By doing this, the different steps in Eq. (8) to count the operations of CM and CA in the RASM can be given respectively as follows:

- $N_r(N+1) + N$ operations of CM and $N_r(N-1) + N_r$ ones of CA are needed in \mathbf{Y} .
- Similar to step 1, $\mathbf{G}_{r,k}$ has $N_r(N+1) + N$ operations of CM but only $N_r(N-1)$ ones of CA.
- The subtraction operation of $\mathbf{Y} - \mathbf{G}_{r,k}$ involves N_r ones of CA.
- In the Frobenius norm, N_r CMS and N_r CAs are needed for calculate the magnitude for each element, and $N_r - 1$ CAs are required in summing the magnitudes.
- In summary, for each set $\{r, k\}$, total complexity can be given as $2N_r(N+2) + N$ of CMs and $2N_r(N-1) + 4N_r - 1$ of CAs.
- Lastly, the total number of all set $\{r, k\}$ is $D \times M$.

Consequently, the total ML detector's operations of CM and CA in the RASM can be obtained as

$$C_{RASM} = [2N_r(2N+1+2N_r) + N-1] DM. \quad (56)$$

As following the same steps of the RASM schemes, $\|\mathbf{Y} - \mathbf{G}_r\|_2^2$ term has the operations of CM and CA in the ML detector applied in the RASSK scheme can be derived as $2N_r(N+2) + N$ and $2N_r(N-1) + 4N_r - 1$, respectively. Differing from the RASM scheme, the total operations of the ML detector in the RASSK scheme can be given as

$$C_{RASSK} = [2N_r(2N+1+2N_r) + N-1] D. \quad (57)$$

Remark 4: In cases where the generalized pre-defined ACs selection is not utilized, D in Eq. (56) and Eq. (57) is replaced into J and $J \gg D$, especially when N_r is large. This leads to a substantial increase in detection complexity, thereby highlighting the significant contribution of the designed ACs selection in reducing complexity.

Remark 5: Comparing the Eq. (56) and Eq. (57), we can find the detection complexity of the RASSK schemes is lower than that of the RASM scheme with the same N_r and N , because the complexity of the detection in constellation symbols is not considered in the RASSK scheme. Also, according to Eq. (56) and Eq. (57), the complexity of both schemes increases with the rise in N_r and N .

Remark 6: In the RSM and RSSK schemes [20], all receive antennas account for channel fading between the transmitter and the RIS and receive signals reflected from the RIS. The CM and CA operations in these schemes are analogous to those in the RASM and RASSK schemes under the same system model configurations, including N and N_r , except for SE. Specifically, the CM and CA operations for RASM and RASSK can be expressed similarly using Eq. (56) and Eq. (57), with D replaced by N_r . This indicates that the complexity of RASM and RASSK approaches that of RSM

and RSSK for small N_r . Nevertheless, the RASM and RASSK schemes achieve higher SE compared to RSM and RSSK with the same N_r . Thus, as the trade-off options applied future wireless networks, we can find that the proposed schemes can yield acceptable complexity and better SE compared to the RSM and RSSK schemes with small N_r .

D. Energy Efficiency Analysis

In addition to SE and BER, energy efficiency (EE) is a paramount metric for evaluating the sustainability of modern wireless communication systems, particularly in IoT scenarios. To mathematically formulate the EE for the proposed schemes, we first define the total power consumption model, denoted as P_{total} . Unlike traditional active MIMO systems that require multiple power-hungry active RF chains at the transmitter, the proposed schemes rely on a single transmit RF chain and a passive RIS array. Therefore, P_{total} can be modeled as:

$$P_{total} = \frac{P_t}{\eta} + P_{TX} + N_r P_{RX} + N P_{RE} + P_{RIS_ctrl}, \quad (58)$$

where P_t is the actual transmit power, and η represents the efficiency of the power amplifier and P_{TX} is the hardware static power consumed by the single RF chain at the transmitter. As all N_r receive antennas remain active to harvest both constructive and non-constructive signals in our schemes, P_{RX} denotes the power consumption per active receive RF chain. For the RIS, P_{RE} represents the near-zero power consumed by each of the N passive reflecting elements for phase shifting, and P_{RIS_ctrl} is the power consumption of the intelligent controller unit. Thus, the EE for the RASM and RASSK schemes can be directly derived by substituting their respective SE from Eq. (21) and Eq. (22) into the EE definition:

$$EE_{RASM} = \frac{[\log_2(2^{N_r} - 1)] + \log_2 M}{\frac{P_t}{\eta} + P_{TX} + N_r P_{RX} + N P_{RE} + P_{RIS_ctrl}}, \quad (59)$$

$$EE_{RASSK} = \frac{[\log_2(2^{N_r} - 1)]}{\frac{P_t}{\eta} + P_{TX} + N_r P_{RX} + N P_{RE} + P_{RIS_ctrl}}. \quad (60)$$

Remark 7: It is critical to highlight that the power consumption of a passive RIS element is significantly lower than that of an active RF chain ($P_{RE} \ll P_{TX}, P_{RX}$). By leveraging the RIS to execute adaptive spatial modulation at the receiver side, the RASM and RASSK schemes effectively map extra information bits without activating additional transmit RF chains. Therefore, the numerator (SE) is substantially enhanced while the denominator (P_{total}) only experiences a marginal increase from the low-power RIS elements. This architectural advantage guarantees that the proposed schemes can achieve superior EE compared to conventional multiple-active-antenna transmission architectures.

V. SYSTEM MODEL AND SECRECY RATE FOR PLS

A. System Model with Eavesdropper

Since the adaptive antenna selection works at a specific receiver in both proposed schemes, the eavesdropper cannot completely detect and decode the received signals from the RIS, which further indicates that the proposed schemes offer

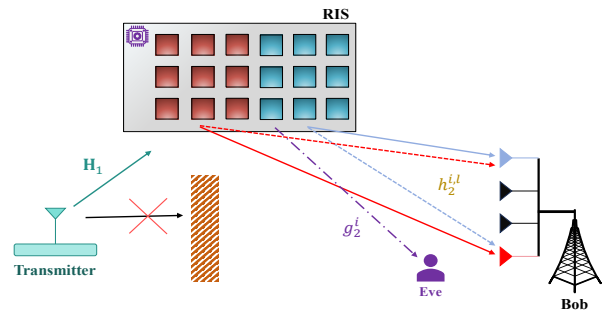


Fig. 2. System model of the RASM and RASSK schemes eavesdropper.

better secrecy performance in terms of PLS during transmission. A new system model in Fig. 2 includes an additional eavesdropper, referred to as Eve equipped with one antenna,⁸ which aims at eavesdropping the transmitted signals from the RIS to the receiver as Bob. It is worth noting that this system model in Fig. 2 is suitable for both the RASM and RASSK schemes, with the only difference that the constellation symbols are transmitted in the RASM scheme instead of the RASSK one. Besides, Eve is assumed to be passive and placed as close to Bob as possible, which means Eve cannot actively attack or interrupt. Here, we also assume that Eve has perfect knowledge of the CSI from the RIS to the receive antenna and the transmitter to the RIS which is given as $g_2 \sim \mathcal{CN}(0, 1)$, following Rayleigh distribution [33]-[35]. Thus, the received signals at Eve can be given as

$$y_e = \sum_{i=1}^N g_2^i \Phi_i h_1^i x_k + \tau_e, \quad (61)$$

where g_2^i and h_1^i bit sequence i -th RE respectively, Φ_i stands for the adjusted phase from the i -th RE, and n_e is the white Gaussian noise with variance N_0 .⁹ The ML detector at Eve is

$$\{\hat{k}\} = \arg \min_k \|y_e - \Delta_e\|_2^2. \quad (62)$$

where $\Delta_e \stackrel{\text{def}}{=} \sum_{i=1}^N g_2^i \Phi_i h_1^i x_k$. In this section, we provide a simple analysis in the SR of the RASM and RASSK schemes.

B. Secrecy Rate Analysis for the RASM Scheme

Referring by [36], the SR of the RASM can be given as

$$R_{RASM} = \max \{0, R_B - R_E\}, \quad (63)$$

where R_B and R_E represent the data rate of Bob and Eve in bpcu, respectively. Note that each selected AC has the same probability as $\frac{1}{D}$ to be chosen to convey bits sequence in a time slot. Thus, by assuming the data rate for all selected ACs are the same, i.e., $R_B^1 = R_B^2 = \dots = R_B^D$ and $R_E^1 = R_E^2 = \dots = R_E^D$, we can easily find that $R_B = R_B^r$ and $R_E = R_E^r$,

⁸Scenarios involving Eve's physical access to the RIS controller or active jamming, e.g., active eavesdropping or jamming attacks, represent different threat models beyond our scope and are not considered.

⁹Since Φ_i is optimized exclusively for Bob's instantaneous channel, it is statistically independent of Eve's channel g_2^i assuming spatial separation. Consequently, Φ_i acts as a random phase value for Eve, precluding any coherent beamforming gain in subsequent derivations.

where R_B^r and R_E^r represent the Bob's and Eve's data rate concerning with r -th selected AC. Thus, the data rate of Bob can be further expressed as

$$R_B = R_B^r + R_B^k, \quad (64)$$

where R_B^r and R_B^k represent the achievable data rate of Bob related to the bits of r -th selected AC and k -th constellation symbol, respectively. On the contrary, Eve has probability in $\frac{1}{D}$ and $\frac{1}{M}$ to successfully guess and decode the ACs and constellation symbols respectively [36]-[37], so the achievable data rate of it can be given as ¹⁰

$$R_E = D^{-1}R_E^r + M^{-1}R_E^k, \quad (65)$$

with R_E^r and R_E^k representing the achievable data rate of Bob related to the bits of r -th selected AC and k -th constellation symbol when Eve successfully decodes both.

According to [36]-[37], the expressions for the achievable data rates of Bob and Eve are given in Eq. (66) and Eq. (67) at the top of the next page, respectively. Detailed proofs can be found in **Appendix A**.

C. Secrecy Rate Analysis for the RASSK Scheme

Similar to Eq. (63), the SR of the RASSK is given as

$$R_{RASSK} = \max \{0, R_B - R_E\}, \quad (68)$$

where $R_B = R_B^r$ and $R_E = 0$ due to the absence of constellation symbols in the RASSK scheme and incapability in detecting the symbols of selected ACs. Furthermore, the mutual information of Bob in the RASSK scheme can be calculated similar to the steps of $\mathfrak{I}_b(k; \mathbf{Y} | h_1^i, h_2^{i,n})$ with replacing x_k into r -th AC in $\Lambda(r)$ and some algebraic calculations, which can be obtained as $R_{RASSK} = \max \{0, R_B\}$, where $R_B = R_B^r$ and $R_E = 0$ due to the absence of constellation symbols in the RASSK scheme and incapability in detecting the symbols of selected ACs. Furthermore, the mutual information of Bob in the RASSK scheme can be calculated similar to the steps of $\mathfrak{I}_b(k; \mathbf{Y} | h_1^i, h_2^{i,n})$ with replacing x_k into r -th AC in $\Lambda(r)$ and some algebraic calculations. Next, taking the expectation of it over h_1^i and $h_2^{i,n}$, R_B can be further expressed as

$$R_B = \log_2 D - \frac{1}{D} \sum_{k=1}^M \sum_{\hat{r}=1}^D \mathbb{E}_{h_1^i, h_2^{i,n}, \tau_n} \left[\log_2 \exp \left(\|\mathbf{N}\|_2^2 - \|\mathbf{Y} - \mathbf{G}_r\| \right) \right]. \quad (69)$$

Substituting Eq. (69) and $R_E = 0$ into $R_{RASSK} = \max \{0, R_B\}$, we can easily find the final SR through Monte Carlo simulations shown in Sec. VI.

Remark 8: Our PLS analysis is rooted in strict information-theoretic secrecy, not obfuscation. Following Kerckhoffs's

¹⁰Total number of possible mapping patterns for constellation symbols and ACs that the transmitter can adopt are M and D , respectively. The probability that Eve adopts the same mapping pattern as the transmitter is $\frac{1}{M}$ for the constellation symbols and $\frac{1}{D}$ for the ACs. This implies that there is only a $\frac{1}{M}$ chance that Eve can correctly guess the exact mapping pattern used by the transmitter for the constellation symbols, and a $\frac{1}{D}$ chance for the ACs.

principle [38], [39], we assume Eve possesses full system knowledge, including the alphabet M , mapping table Λ , and RIS strategy. Security fundamentally stems from spatial channel decorrelation: the RIS passive beamforming is exclusively aligned to the legitimate cascaded channel. Consequently, an eavesdropper at a different location experiences an independent, unaligned channel. This physical disparity inherently degrades Eve's mutual information and guarantees a positive secrecy rate, completely independent of her knowledge of the mapping rules.

Remark 9: The RIS phase shifts are strictly optimized for the legitimate cascaded channel. Consequently, even if an eavesdropper intercepts high signal energy, their independent cascaded channel scrambles the delicate energy differences and phase alignments required to decode the spatial activation cues, rendering statistical blind estimation ineffective. This evaluation assumes the ubiquitous condition of independent fading, e.g., $d \gg \lambda/2$. However, if the eavesdropper is located in extreme proximity to the legitimate receiver ($d < \lambda/2$), their channels become highly spatially correlated. Under such specific conditions, significant information leakage is inevitable a fundamental physical limitation governed by electromagnetic wave propagation that is intrinsic to all spatial-domain physical layer security architectures.

VI. SIMULATION RESULTS

In this section, the analytical and simulation results are presented. To provide a more comprehensive illustration of the performance in the proposed scheme, a uniform assumption of Rayleigh channel fading is adopted, **except for Fig. 6**, with the transmission antenna $N_t = 1$ to be considered in all cases of the RASM and RASSK schemes. All of these results are conducted by employing the Monte Carlo simulations, encompassing a substantial number of channel realizations, precisely 3×10^6 . Similar to [14]-[18], $\bar{\gamma} = \frac{E_s}{N_0}$ is considered as the average SNR at receiver.

The analytical and simulation results of BER in the RASM scheme are presented in Fig. 3, where the results of the cases with $N_r = 4$ and 5, $N = 8$ and 16, $M = 2$ and 4 are given, respectively. As depicted in Fig. 3, BER decreases monotonically with an increase in N . This trend underscores the significant impact of the RIS in enhancing BER performance. For the case with $N_r = 4$, $N = 16$, and $M = 2$, we can find that the BER of the RASM scheme is lower than 10^{-5} when SNR is equal to 10 dB and bpcu is equal to 4, which indicates the proposed scheme can achieve the desired BER performance. ¹¹ Particularly as the SNR increases, the simulation results closely approach to the theoretical ones, which is mainly because of the applications of CLT in theoretical analysis. Additionally, the gap between the theoretical and simulation results decreases as N increases. This is also because the CLT utilization, causing the theoretical BER to converge with the simulations as N grows. We can observe that the BER performance worsens as N_r increases, which is because the increase in N_r leads to the increase in

¹¹Since the analytical curves represent theoretical upper bounds derived via the Union Bound technique, these bounds naturally become loose and may mathematically exceed 0.5 in the low-SNR regime due to the summation of overlapping pairwise error probabilities.

$$R_B = \log_2 DM - \frac{1}{DM} \sum_{r=1}^D \sum_{k=1}^M \mathbb{E}_{h_1^i, h_2^i, \tau_n} \left\{ \log_2 \left[1 + \sum_{\hat{r}=1, \hat{r} \neq r}^D \sum_{\hat{k}=1, \hat{k} \neq k}^M \exp \left(-\|Y - G_{r,k}\|_2^2 + N \right) \right] \right\}. \quad (66)$$

$$R_E = \frac{1}{M} \left\{ \log_2 M - \frac{1}{M} \sum_{k=1}^M \mathbb{E}_{n_e, g_1^i, g_2^i} \left[\log_2 \frac{1 + \exp \left(-\|\tau_e\|_2^2 \right)}{\sum_{\hat{k}=1}^M \left[1 + \exp \left(-\|y_e - \sum_{i=1}^N g_2^i \Phi_i g_1^i x_{\hat{k}}\|_2^2 \right) \right]} \right] \right\}. \quad (67)$$

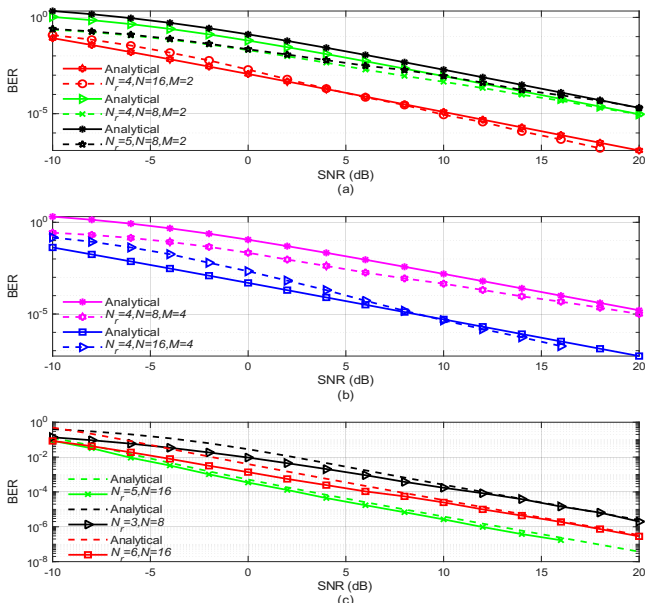


Fig. 3. Analytical and simulation BER results of the RASM in (a) and (b), and RASSK schemes in (c).

number of ACs, thus leading to increase error possibility in detection. For the same reason, by comparing the results of $M = 2$ and $M = 4$ between (a) and (b) in Fig. 3, the slight discrepancy and learn that the BER performance deteriorates with the increase of M . Fig. 3 (c) illustrates the analytical and simulation BER performance of the RASSK scheme, where $N_r = 3, 5, 6$ and $N = 8, 16$, respectively. Similar to (a) and (b), we learn from (c) that BER performance of the RASSK scheme gets better with the increase of SNR and the analytical BER is approached to the simulation one especially in the higher SNR range. Additionally, the results in (c) also point out that the RASSK has satisfactory BER performance even under the low SNR situation.

Since all of receive antennas are required to receive signals in the received IM schemes, the BER performance gets better with the increase of N_r . We only need N_d receive antennas to implement the RASSK-based in antenna selection for the same SE condition during comparisons.¹² Note that $N_r = 16$ is assumed in all received IM schemes of Fig. 4. For fair

¹² N_d closely related to SE, which can be easily obtained from Eq. (21)-Eq. (26) by replacing N_r into N_d . $N_d \neq N_r$ is only given in Fig. 4. For convenience, we assume $N_d = N_r$ in other figures.

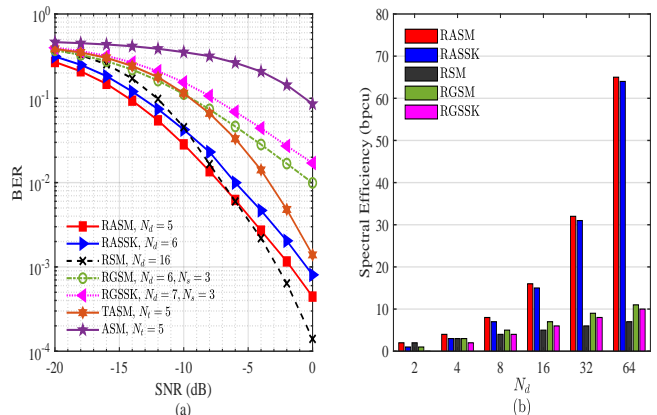


Fig. 4. (a) BER performance and (b) spectral efficiency represented by bpcu of various IM schemes with different N_d , $N_r = 16$, $M = 2$, and $N = 8$.

comparison, bpcu of all schemes in Fig. 4 (a) is 5, and $N = 8$ is given in all schemes of Fig. 4. Also, $M = 2$ is for the RASM, RSM, and RGSM schemes. Thus, the RASM scheme has $N_d = 5$, the RASSK scheme has $N_d = 6$, the RSM scheme has $N_d = 16$, the RGSM scheme has $N_d = 6$ and $N_s = 3$, and the RGSSK scheme has $N_d = 3$ and $N_s = 3$, where N_s represents the number of selected antennas in the RGSM and RGSSK schemes [22]-[23]. Plus, by comparing the BER performance of the TASM and ASM scheme with generalized pre-defined ACs selection, the BER performance of the RASM scheme significantly outperforms that of the TASM and ASM scheme. The reason lies in the fact that within the TASM scheme, the AC indices undergo dual-stage channel fading, contrasting with the single stage in the RASM scheme, while additionally lacking the support provided by the RIS in the ASM scheme. According to Fig. 4 (a), we find that the BER performance of the RASM and RASSK schemes is better than that of the RGSM and RGSSK schemes. Furthermore, the BER performance of the RASM and RASSK schemes is worse than that of the RSM scheme when SNR is larger than around -2 dB in the RASM scheme and around -10 dB in the RASSK scheme. However, the BER performance of the RASM and RASSK schemes is better than that of the RSM when SNR is lower than about -2 dB, where the BER performance of the proposed schemes are apparently better with large N and increased M . In comparison between the RASM and RASSK schemes, we can find that the BER performance of the RASM scheme is better than that of the RASSK, evidencing that

the constellation-symbol modulation outperforms the received ACs-selection modulation in the receive IM scheme. On the other hand, with the increase of N_d , the bpcu of the RASM and RASSK schemes have a significant improvement and is tremendously higher than other schemes especially with the high N_d , which further indicates the proposed scheme can provide higher SE in wireless transmission. Since the constellation symbol is not transmitted in the RASSK scheme, the RASM scheme always has 1 bpcu higher than the RASSK scheme when $M = 2$, as shown in Fig. 4 (b).

Giving the same condition on SE, the comparison of the various received RIS-assisted IM schemes with the imperfect CSI estimation is shown in Fig. 5, where the schemes include the RASM, RASSK, and RSM schemes. Here, the imperfect CSI is assumed in $h_2^{i,m}$ with δ^2 in the RTSM and RTSSK schemes representing the variance of estimation error [40]-[41] and the spectral efficiency is $R = 4$ bpcu. Detail explanations of the imperfect CSI estimation can be found in Appendix B. Results in Fig. 5 show that the robustness of the RASSK scheme is better than that of the RASM and RSM schemes, despite the fact that the δ^2 in the RASSK results is larger than others. Also, the BER performance of RASM scheme outperforms the one of the RSM scheme. Furthermore, when facing hardware-induced phase quantization errors ($b = 3$), the RASSK scheme exhibits exceptional resilience, with its BER continuously dropping below 10^{-3} at low SNR regions. In contrast, the RASM scheme experiences a noticeable performance floor. This performance gap physically reveals that conveying information purely through received power at selected antennas (as in RASSK) is inherently more robust to phase mismatches than detecting conventional M -ary constellation symbols (as in RASM). According to these comprehensive comparisons, it can be firmly concluded that the proposed RASSK scheme holds immense potential for applications in complex and imperfect real-world wireless environments due to its superior robustness against both CSI estimation inaccuracies and hardware phase quantization errors.

Fig. 6 shows BER of RASM scheme with $N_r = 8, N_d = 4, N = 32$, and $M = 2$, RASSK scheme with $N_r = 8$ and $N_d = 5$, RSM scheme with $N_r = 8, N = 32$, and $M = 2$, of which the $K = 5, 10$, and 15 , respectively. In Fig. 6, we can find that the BER performance of all schemes gets worse with the increase of K . This is because stronger LoS component makes the channel responses at different antennas more similar. When receive antennas are closely spaced, their channel characteristics become very similar, thus reducing spatial diversity. Since IM schemes, especially the SM and SSK related schemes, rely on distinct channel characteristics for correct detection of antenna indices, this reduced diversity leads to degrade BER performance. This phenomenon is particularly evident in the results of RASSK scheme shown in Fig. 6, which further corroborates the aforementioned argument. However, the BER performance of RASM scheme still outperforms the one of RSM scheme even with different K . As shown in Fig. 6, RASM consistently outperforms RSM across varying K . This stems from RASM's adaptive antenna activation, which generates richer spatial signatures and allows a lower constellation order, thereby increasing the minimum

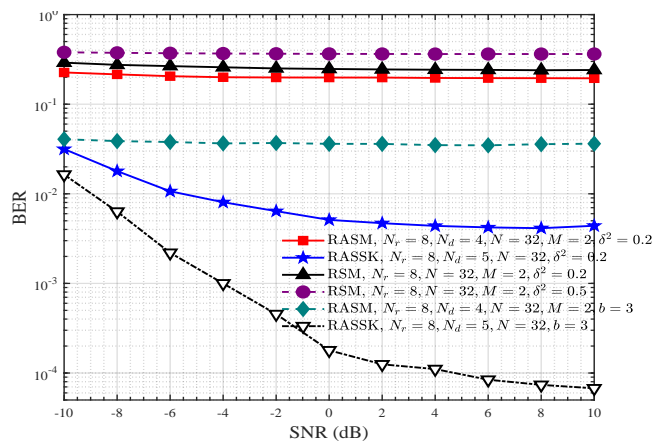


Fig. 5. BER performance of the RASM, RASSK, and RSM schemes with imperfect CSI estimation and quantized RIS phase errors.

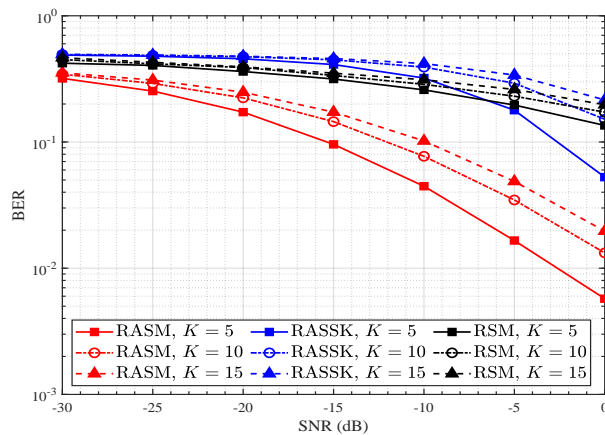


Fig. 6. BER performance of the RASM, RASSK, and RSM schemes with Rician channel fading in \mathbf{H}_2 .

Euclidean distance. Also, the RIS phases are optimized based on the instantaneous cascaded CSI, which includes both LoS and Rayleigh components, constructively harvesting Rayleigh energy. Optimizing solely for the LoS path would leave the unaligned Rayleigh component as severe interference.

Fig. 7 shows the SR of the RASM and RASSK schemes. First, Fig. 7 shows that the SR of both schemes gets better with the increase of the SNR. Nevertheless, we can also observe that the increase rate stabilizes across all results within the high SNR regime. With the N increasing, the SR of the RASM scheme with $N_r = 3, N = 8$, and $M = 2$ is slightly worse than that with $N = 16$, which shows the increase of N can improve the PLS performance due to the enhancement in SNR at receiver. In addition, by comparing the results of the RASM scheme with different bpcu, i.e., $N_r = 3, 4$ and $M = 2, 4$, the SR increases while the bpcu increasing, thus the higher SE provides better PLS performance in the RASM scheme. Specifically, the SR of the RASM scheme with $N_r = 3, N = 16$, and $M = 2$ is worse than that of the one with $N_r = 4, N = 16$, and $M = 4$, which not only can be learned from the theoretical analysis in Sec. IV where the R_E decreases with the increase in M due to the $\frac{1}{M}$ term in Eq. (75), but also demonstrates the higher-order modulation is more capable of

enhancing the data rate with the assistance of the RIS than the ACs indices. For the RASSK scheme, since it only transmits bits mapped from the ACs selection, the entire signal cannot be successfully detected by Eve. Thus, the SR of the RASSK is higher than that of the RASM scheme, which can be obtained by comparing the results of the RASSK scheme and the RASM scheme of the Fig. 7 (a) and (b), respectively. As also given in Fig. 7, it is clear that the SR of the RASSK scheme also increases with the rise of SNR and N_r . In contrast to the RASM scheme, the increase rate of SR in the RASSK scheme starts to level off when SNR < 0 dB, which also can indicate the superiority in PLS of the RASSK scheme.

Following model of MRC in [42], the SR of the RIS-assisted SIMO scheme with MRC (SIMO-MRC), the TSM scheme with MRC (TSM-MRC), the TSM-MRC with AN¹³, and the TSSK scheme with MRC (TSSK-MRC) are given to compare with the one in both proposed schemes as shown in Fig. 7.¹⁴ To make a fair comparison, as the same SE in 3 bits/s/Hz, the RASM has $N_r = 4$, $N = 8$, $M = 2$, and the RASSK has $N_r = 4$, $N = 8$, and the SIMO-MRC has $N_t = 1$, $N_r = 3$, $N = 8$, $M = 32$, and the TSM-MRC scheme has $N_t = 3$, $N_r = 3$, $N = 8$, $M = 2$, and the TSSK-MRC scheme has $N_t = 8$, $N_r = 3$, $N = 8$. In Fig. 7, the SR of both proposed schemes is higher than that of the others from -30 dB to 30 dB, demonstrating that the received IM schemes achieve better PLS performance compared to the traditional SIMO-MRC, TSM-MRC, and TSSK-MRC schemes, even the PLS wireless technique, e.g., AN in the TSM-MRC. Below around -5 dB, the SR of the SIMO-MRC scheme is slightly higher than that of TSM-MRC and TSSK-MRC, indicating that the PLS performance based on transmit antenna indices is weaker than that based on constellation symbols. The SR results of TSM-MRC and TSSK-MRC are closed because Bob and Eve share the same transmitter-to-RIS channel, and the CSI is assumed to be known to Eve, allowing her to fully detect and decode the transmitted signals, which is a limitation of transmitted IM schemes. Notably, the SR of the SIMO-MRC, TSM-MRC, and TSSK-MRC schemes approaches but does not reach zero, as Bob's channel capacity remains higher than Eve's due to having multiple antennas, while Eve only has one.

Remark 10: Achieving symbol-level RIS reconfiguration demands strict synchronization, as timing failures can cause severe phase misalignment and substantial BER degradation, which is a non-trivial issue and out of our scope, thus leaving for future works. Regarding hardware complexity, both the proposed RASM and conventional fixed-antenna schemes, e.g., RSM, RGSM, and RGSSK, fundamentally require all N_r receive antennas to be connected to active RF chains for spatial detection. Therefore, our adaptive mechanism introduces no additional RF hardware cost at the receiver. This receiver-centric complexity is a deliberate design trade-off, enabling a

¹³This AN is designed with the noise variance N_0 as the same to the Gaussian white noise. Detail AN model can be found in [43].

¹⁴Since there is currently no existing literature discussing and investigating the PLS performance of the TASM scheme, where the adaptive antenna selection works at transmitter and the RIS is employed as a passive relay, we thus select the TSM and TSSK schemes as benchmarks to compare the SR with both proposed schemes in this paper.

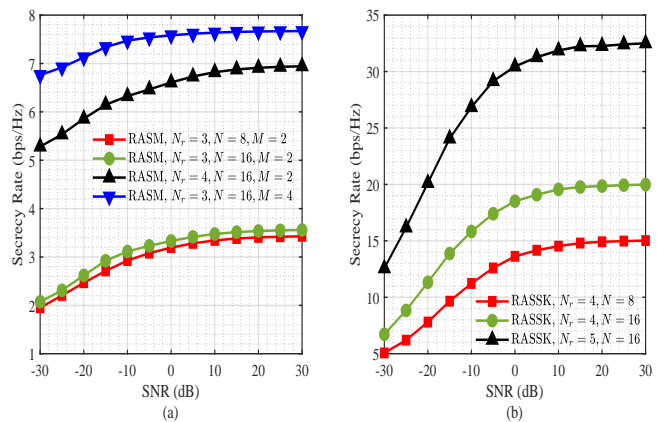


Fig. 7. (a) SR of the RASM scheme and (b) the RASSK scheme, with $N_r = 3, 4$, and 5, $N = 8$ and 16, $M = 2$ and 4.

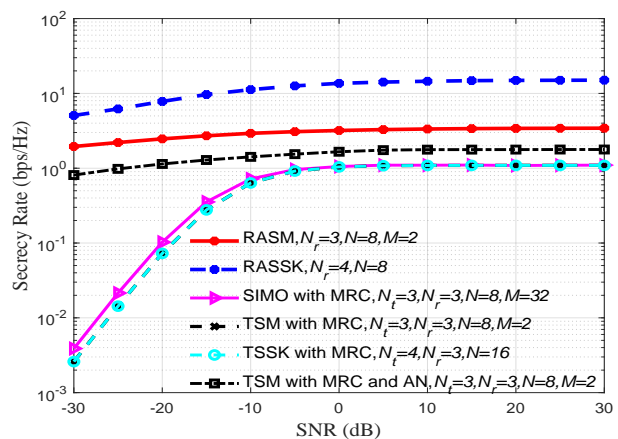


Fig. 8. SR of the RASM and RASSK schemes compared to the RIS-assisted SIMO, TSM, TSSK schemes empowered by the MRC with $N_r = 3$ and 4, $N_t = 1, 4$, and 8, $M = 2$ and 32, $N = 8$, and AN.

minimalist, single-RF-chain architecture for power-constrained IoT transmitters.

VII. CONCLUSION

This paper presented two novel RIS-assisted IM schemes, RASM and RASSK, aimed at enhancing SE and ensuring PLS in wireless transmissions. When the number of receive antennas is 8 or more, the proposed scheme achieves approximately twice the SE of the traditional RSM scheme, while only providing an SNR loss of around 0.5 dB at a target BER lower than 10^{-3} . Moreover, our physical layer security evaluations confirm that the spatial channel decorrelation inherent to our design strictly guarantees a positive secrecy rate, thoroughly validating the system's robustness against unauthorized eavesdropping. To further approach practical applications, more sophisticated eavesdropper models, as well as the evaluation of the proposed schemes in dynamic multi-user environments with high mobility, will be considered in our future works. Overall, these schemes showed strong potential for future wireless applications.

REFERENCES

- [1] C. Zhang, H. Xu, B. Ng, and Chan-Tong Lam, "RIS-Assisted Received Adaptive Spatial Modulation for Wireless Communication," arxiv: 2407.06894, Jul., 2024.

- [2] J. Jeganathan, A. Ghrayeb, L. Szczecinski and A. Ceron, "Space shift keying modulation for MIMO channels," *IEEE Trans. Wireless Commun.*, vol. 8, no. 7, pp. 3692-3703, Jul. 2009.
- [3] J. Jeganathan, A. Ghrayeb, and L. Szczecinski, "Generalized space shift keying modulation for MIMO channels," in *Proc. IEEE Int. Symp. Pers., Indoor Mobile Radio Commun.*, Cannes, France, 2008, pp. 1-5.
- [4] P. Yang, Y. Xiao, Y. Yu and S. Li, "Adaptive spatial modulation for wireless MIMO transmission systems," *IEEE Commun. Lett.*, vol. 15, no. 6, pp. 602-604, Jun. 2011.
- [5] C. Pan et al., "An overview of signal processing techniques for RIS/IRS-aided wireless systems," *IEEE J. Sel. Topics Signal Process.*, vol. 16, no. 5, pp. 883-917, Aug. 2022.
- [6] K. Wang, C. -T. Lam and B. K. Ng, "How long can RIS work effectively: An electronic reliability perspective," in *Proc. IEEE 98th Veh. Technol. Conf. (VTC-Fall)*, Oct. 2023, pp. 1-6.
- [7] Q. Wu, S. Zhang, B. Zheng, C. You and R. Zhang, "Intelligent reflecting surface-aided wireless communications: A tutorial," *IEEE Trans. Commun.*, vol. 69, no. 5, pp. 3313-3351, May 2021.
- [8] W. Tang et al., "Wireless communications with reconfigurable intelligent surface: Path loss modeling and experimental measurement," *IEEE Trans. Wirel. Commun.*, vol. 20, no. 1, pp. 421-439, Jan. 2021.
- [9] K. An et al., "Exploiting multi-layer refracting RIS-assisted receiver for HAP-SWIPT networks," *IEEE Trans. Wireless Commun.*, vol. 23, no. 10, pp. 12638-12657, Oct. 2024.
- [10] Z. Lin et al., "Refracting RIS-aided hybrid satellite-terrestrial relay networks: Joint beamforming design and optimization," *IEEE Trans. Aerosp. Electron. Syst.*, vol. 58, no. 4, pp. 3717-3724, Aug. 2022.
- [11] L. Zhi et al., "Self-powered absorptive reconfigurable intelligent surfaces for securing satellite-terrestrial integrated networks," *China Commun.*, vol. 21, no. 9, pp. 276-291, Sep. 2024.
- [12] Z. Lin et al., "Wireless endogenous security for SAGINs: Achieving ubiquitous access and secure communication in symbiosis," *IEEE Netw.*, vol. 39, no. 6, pp. 155-163, Nov. 2025.
- [13] B. Zheng, C. You, W. Mei and R. Zhang, "A survey on channel estimation and practical passive beamforming design for intelligent reflecting surface aided wireless communications," *IEEE Commun. Surveys Tuts.*, vol. 24, no. 2, pp. 1035-1071, 2nd quarter 2022.
- [14] A. E. Canbilen, E. Basar, and S. S. Ikki, "Reconfigurable intelligent surface-assisted space shift keying," *IEEE Wirel. Commun. Lett.*, vol. 9, no. 9, pp. 1495-1499, Sept. 2020.
- [15] Q. Li, X. Lin, C. Zhang and J. Li, "Novel RIS-aided receive spatial modulation via joint active and passive beamforming," *IEEE Wirel. Commun. Lett.*, vol. 13, no. 4, pp. 1058-1062, April 2024.
- [16] A. Bhowal, S. Aïssa and R. Singh Kshetrimayum, "RIS-assisted spatial modulation and space shift keying for ambient backscattering communications," in *Proc. IEEE Int. Conf. Commun.*, 2021, pp. 1-6.
- [17] M. Yue, Y. Peng, R. Ye and J. Lee, "STAR-RIS assisted ambient backscatter communication system with index modulation," *IEEE Trans. Veh. Technol.*, vol. 74, no. 8, pp. 13231-13236, Aug. 2025.
- [18] Q. Jin, Y. Peng, F. Al-Hazemi, and J. Lee, "A pattern modulation based IRS scheme for space shift keying communication system," *IEEE Commun. Lett.*, vol. 28, no. 6, pp. 1417-1421, Jun. 2024.
- [19] Q. Li, M. El-Hajjar, Y. Sun, and L. Hanzo, "Performance analysis of reconfigurable holographic surfaces in the near-field scenario of cell-free networks under hardware impairments," *IEEE Trans. Wireless Commun.*, vol. 23, no. 9, pp. 11972-11984, Sep. 2024.
- [20] X. Zhu, Q. Wu, and W. Chen, "Transmissive RIS transmitter enabled spatial modulation MIMO systems," *IEEE J. Sel. Areas Commun.*, vol. 43, no. 3, pp. 899-911, Mar. 2025.
- [21] E. Basar, "Reconfigurable intelligent surface-based index modulation: A new beyond MIMO paradigm for 6G," *IEEE Trans. Commun.*, vol. 68, no. 5, pp. 3187-3196, May 2020.
- [22] H. Albinsaid, K. Singh, A. Bansal, S. Biswas, C. -P. Li, and Z. J. Haas, "Multiple antenna selection and successive signal detection for SM-based IRS-aided communication," *IEEE Signal Process. Lett.*, vol. 28, pp. 813-817, Apr. 2021.
- [23] C. Zhang, Y. Peng, J. Li, and F. Tong, "An IRS-aided GSSK scheme for wireless communication system," *IEEE Comm. Lett.*, vol. 26, no. 6, pp. 1398-1402, Jun. 2022.
- [24] L. Xiong, Y. Peng and J. Lee, "A partitioned-IRS assisted transmit GSSK scheme for wireless communication system," *IEEE Wirel. Commun. Lett.*, vol. 13, no. 2, pp. 260-264, Feb. 2024.
- [25] C. Zhang and Y. Peng, "Received antenna array design of GSSK-based antennas selection for RIS-assisted communication," *IEEE Syst. J.*, vol. 17, no. 2, pp. 3366-3369, June 2023.
- [26] X. Cai, C. Huang, P. Chen, E. Basar, and C. Yuen, "Design of non-coherent RIS-empowered DCSK with two-level nested index modulation," *IEEE Trans. Wireless Commun.*, vol. 24, no. 4, pp. 3044-3058, Apr. 2025.
- [27] X. Cai et al., "Toward RIS-aided non-coherent communications: A joint index keying M-ary differential chaos shift keying system," *IEEE Trans. Wireless Commun.*, vol. 22, no. 12, pp. 9045-9062, Dec. 2023.
- [28] X. Cai, C. Yuen, C. Huang, W. Xu, and L. Wang, "Toward chaotic secure communications: An RIS enabled M-ary differential chaos shift keying system with block interleaving," *IEEE Trans. Commun.*, vol. 71, no. 6, pp. 3541-3558, Jun. 2023.
- [29] T. Ma, Y. Xiao, X. Lei, P. Yang, X. Lei and O. A. Dobre, "Large intelligent surface assisted wireless communications with spatial modulation and antenna selection," *IEEE J. Sel. Areas Commun.*, vol. 38, no. 11, pp. 2562-2574, Nov. 2020.
- [30] Y. Liu, C. Zhang, B. K. Ng and C. -T. Lam, "RIS-assisted dual-polarized spatial modulation with CVCNN-based detector," *IEEE Wirel. Commun. Lett.*, vol. 14, no. 9, pp. 2942-2946, Sept. 2025.
- [31] H. Albinsaid, K. Singh, S. Biswas, C. -P. Li and M. -S. Alouini, "Block deep neural network-based signal detector for generalized spatial modulation," *IEEE Comm. Lett.*, vol. 24, no. 12, pp. 2775-2779, Dec. 2020.
- [32] L. Xiao et al., "A low-complexity detection scheme for differential spatial modulation," *IEEE Comm. Lett.*, vol. 19, no. 9, pp. 1516-1519, Sept. 2015.
- [33] J. Wang, S. Wang, S. Han and C. Li, "Intelligent reflecting surface secure backscatter communication without eavesdropping CSI," *IEEE Comm. Lett.*, vol. 27, no. 6, pp. 1496-1500, Jun. 2023.
- [34] J. Jian, W. -Q. Wang, A. Basit and B. Huang, "Physical layer security for frequency diverse array-based dual-hop spatial modulation," *IEEE Trans. Wireless Commun.*, vol. 22, no. 11, pp. 7565-7579, Nov. 2023.
- [35] J. -Y. Wang, H. Ge, M. Lin, J. -B. Wang, J. Dai and M. -S. Alouini, "On the secrecy rate of spatial modulation-based indoor visible light communications," *IEEE J. Sel. Areas Commun.*, vol. 37, no. 9, pp. 2087-2101, Sept. 2019.
- [36] U. Singh, M. R. Bhatnagar and T. A. Tsiftsis, "Secrecy analysis of SSK modulation: adaptive antenna mapping and performance results," *IEEE Trans. Wireless Commun.*, vol. 20, no. 7, pp. 4614-4630, Jul. 2021.
- [37] U. Singh and M. R. Bhatnagar, "Secrecy analysis for spatial modulation: Transmission scheme and performance evaluation," *IEEE Comm. Lett.*, vol. 26, no. 1, pp. 35-39, Jan. 2022.
- [38] A. Kerckhoffs, "La cryptographie militaire," *Journal des sciences militaires*, vol. 9, pp. 5-38, Jan. 1883.
- [39] C. E. Shannon, "Communication theory of secrecy systems," *The Bell System Technical Journal*, vol. 28, no. 4, pp. 656-715, Oct. 1949.
- [40] S. Saini and A. Chockalingam, "Performance of RIS-aided media-based modulation with imperfect CSI and phase tuning errors," in *Proc. PIMRC*, Toronto, ON, Canada, 2023, pp. 1-6.
- [41] P. Yang, L. Yang and S. Wang, "Performance analysis for RIS-aided wireless systems with imperfect CSI," *IEEE Wirel. Commun. Lett.*, vol. 11, no. 3, pp. 588-592, Mar. 2022.
- [42] F. Zhou, X. Li, M. Alazab, R. H. Jhaveri and K. Guo, "Secrecy performance for RIS-based integrated satellite vehicle networks with a UAV relay and MRC eavesdropping," *IEEE Trans. Intell. Veh.*, vol. 8, no. 2, pp. 1676-1685, Feb. 2023.
- [43] S. Arzykulov, A. Celik, G. Nauryzbayev and A. M. Eltawil, "Artificial noise and RIS-aided physical layer security: Optimal RIS partitioning and power control," *IEEE Wirel. Commun. Lett.*, vol. 12, no. 6, pp. 992-996, Jun. 2023.

APPENDIX A

The mutual information of Bob and Eve are derived. The achievable data rate for Bob and Eve can be obtained as a discrete-input continuous-output memoryless channel (DCMC) capacity [36]-[37]. For the RASM scheme, mutual information of Bob can be obtained as:

$$\mathfrak{I}_b(k, r; \mathbf{Y}|\mathbf{H}_1, \mathbf{H}_2) = \mathfrak{I}_b(k; \mathbf{Y}|\mathbf{H}_1, \mathbf{H}_2) + \mathfrak{I}_b(r; \mathbf{Y}|\mathbf{H}_1, \mathbf{H}_2, k), \quad (70)$$

where y_m represents the received signal at m -th receive antenna, $\mathfrak{I}_b(k; \mathbf{Y}|\mathbf{H}_1, \mathbf{H}_2)$ represents the mutual information between \mathbf{Y} and x_k , $\mathfrak{I}_b(r; \mathbf{Y}|\mathbf{H}_1, \mathbf{H}_2, k)$ stands for the mutual information between \mathbf{Y} and r -th AC after AC selection when

x_k is given. $\mathfrak{I}_b(k; \mathbf{Y} | \mathbf{H}_1, \mathbf{H}_2)$ can be further expressed as:

$$\begin{aligned} \mathfrak{I}_b(k; \mathbf{Y} | \mathbf{H}_1, \mathbf{H}_2) &= \sum_{k=1}^M \int P_r(x_k) f(\mathbf{Y} | k) \log_2 \frac{f(\mathbf{Y} | k)}{f(\mathbf{Y})} d\mathbf{Y}, \quad (71) \end{aligned}$$

where $P_r(x_k) = \frac{1}{M}$ since each constellation symbol is selected equiprobably, which is the same in each AC equiprobably selected in $\Lambda(r)$ as $P_r(r) = \frac{1}{D}$. And the PDF of \mathbf{Y} and the conditional PDF of \mathbf{y} when k is given are $f(\mathbf{Y}) = \sum_{r=1}^D \sum_{k=1}^M \frac{e^{-\|\mathbf{Y} - \mathbf{G}_{r,k}\|_2^2}}{DM\pi^{N_a}}$ and $f(\mathbf{Y} | k) = \frac{1}{D} \sum_{r=1}^D \frac{e^{-\|\mathbf{Y} - \mathbf{G}_{r,k}\|_2^2}}{D\pi^{N_a}}$, respectively. By substituting $f(\mathbf{Y})$ and $f(\mathbf{Y} | k)$ into (65) and after some algebra, the mutual information between y_l and x_k can be rewritten as

$$\begin{aligned} \mathfrak{I}_b(k; \mathbf{Y} | \mathbf{H}_1, \mathbf{H}_2) &= \log_2 M - \\ &\frac{1}{DM} \sum_{r=1}^D \sum_{k=1}^M \sum_{\hat{r}=1}^D \sum_{\hat{k}=1}^M \mathbb{E}_{\tau_n} \left[\log_2 e^{\|\mathbf{Y} - \mathbf{G}_{\hat{r},\hat{k}}\|_2^2 - \|\mathbf{Y} - \mathbf{G}_{r,k}\|_2^2} \right]. \quad (72) \end{aligned}$$

Also, the mutual information between y_l and r -th AC in $\Lambda(r)$ when x_k is given can be obtained as:

$$\begin{aligned} \mathfrak{I}_b(r; \mathbf{Y} | \mathbf{H}_1, \mathbf{H}_2, k) &= \sum_{r=1}^D \sum_{k=1}^M \int f(k, r) f(\mathbf{y} | k, r) \log_2 \frac{f(\mathbf{y} | k, r)}{f(\mathbf{y} | k)} dy_l, \quad (73) \end{aligned}$$

where $f(k, r)$ represents a joint PDF of x_k and r -th AC in $\Lambda(r)$ as a product of their individual PDFs which follows the uniform distribution function, and $f(\mathbf{y} | k, r)$ denotes the conditional PDF of \mathbf{y} when k and r are given as:

$$f(\mathbf{Y} | k, r) = \frac{1}{\pi^{N_a}} \exp\left(-\|\mathbf{N}\|_2^2\right). \quad (74)$$

Substituting $f(\mathbf{Y} | k)$ and Eq. (73) into Eq. (71), the mutual information between y_l and r -th AC in $\Lambda(r)$ is:

$$\begin{aligned} \mathfrak{I}_b(r; \mathbf{Y} | \mathbf{H}_1, \mathbf{H}_2, k) &= \log_2 D - \\ &\frac{1}{DM} \sum_{r=1}^D \sum_{k=1}^M \mathbb{E}_{\tau_n} \left[\log_2 \sum_{r=1}^D e^{-\|\mathbf{Y} - \mathbf{G}_{r,k}\|_2^2 + \mathbf{N}} \right]. \quad (75) \end{aligned}$$

By taking expectation of Eq. (75) and Eq. (77) over h_1^i and $h_2^{i,m}$, R_B^r and R_B^k can be obtained respectively. Finally, according to Eq. (64), the data rate of Bob can be written as Eq. (66). Since Eve only can detect the constellation symbols of the transmitted signals, we can consider that $R_E^r = 0$, thus the Eq. (65) can be further rewritten as $R_E = \frac{1}{M} R_E^k$. Besides, assuming both Eve and Bob can perfectly detect the constellation symbols, the mutual information of Eve is similar to $\mathfrak{I}_b(k; y_l | h_1^i, h_2^{i,l})$ as given in Eq. (71), which can be derived as follows:

$$\mathfrak{I}_e(k; y_e | g_1^i, g_2^i) = \sum_{k=1}^M \int P_r(x_k) f(y_e | k) \log_2 \frac{f(y_e | k)}{f(y_e)} dy_e, \quad (76)$$

with $f(y_e | k) = \frac{1}{\pi} \exp\left(-\|\tau_e\|_2^2\right)$ and

$$f(y_e) = \frac{1}{M} \sum_{k=1}^M \frac{1}{\pi} \exp\left(-\left\|y_e - \sum_{i=1}^N g_2^i \Phi_i h_1^i x_k\right\|_2^2\right). \quad (77)$$

Then, by taking expectation of Eq. (77) over g_1^i and g_2^i and multiplying $\frac{1}{M}$, we can obtain the achievable data rate of Eve as Eq. (67).

APPENDIX B

The CSI estimation at receiver can hardly be perfect especially in complex wireless environment. For simplicity, the imperfect CSI estimation is only considered in the channel from the RIS to receive. According to this and referring to the imperfect CSI model from [40], [41], the coefficient of $\check{h}_2^{i,m}$ can be expressed as the sum of $\check{h}_2^{i,m} \sim \mathcal{CN}(0, 1 - \delta_{e1}^2)$ and $\check{h}_2^{i,m} \sim \mathcal{CN}(0, \delta_{e1}^2)$. Giving that δ_{e2}^2 denotes the inaccuracy of estimation in CSI with $\delta_{e2}^2 = 1 - \delta_{e2}^2$. Thus, we can respectively obtain the receive signals at l -th receive antenna in r -th selected AC for the RASM and RASSK schemes with imperfect CSI estimation as

$$\begin{aligned} \check{y}_l^{RASM} &= \underbrace{\sum_{i=(l-1)N_E+1}^{zN_E} \left(\delta_{e2}^2 \check{h}_2^{i,m} + \delta_{e2}^2 \check{h}_2^{i,m} \right) \Phi_{i,l} h_1^i x_k}_{\text{constructive part}} \\ &\quad + \underbrace{\sum_{q=1, q \neq l}^{N_a} \sum_{i=(q-1)N_E+1}^{qN_E} \left(\delta_{e2}^2 \check{h}_2^{i,m} + \delta_{e2}^2 \check{h}_2^{i,m} \right) \Phi_{i,l} h_1^i x_k + \tau_l}_{\text{non-constructive part}}, \quad (78) \end{aligned}$$

$$\begin{aligned} \check{y}_l^{RASSK} &= \sqrt{E_s} \underbrace{\sum_{i=(l-1)N_E+1}^{zN_E} \left(\delta_{e2}^2 \check{h}_2^{i,m} + \delta_{e2}^2 \check{h}_2^{i,m} \right) \Phi_{i,l} h_1^i}_{\text{constructive part}} \\ &\quad + \underbrace{\sqrt{E_s} \sum_{q=1, q \neq l}^{N_a} \sum_{i=(q-1)N_E+1}^{qN_E} \left(\delta_{e2}^2 \check{h}_2^{i,m} + \delta_{e2}^2 \check{h}_2^{i,m} \right) \Phi_{i,l} h_1^i + \tau_l}_{\text{non-constructive part}}. \quad (79) \end{aligned}$$

In the meanwhile, the received signals with imperfect CSI estimation of u -th unselected receive antenna in the RASM and RASSK schemes can be respectively given as:

$$\begin{aligned} \check{y}_u^{RASM} &= \sum_{q=1}^{N_a} \sum_{i=(q-1)N_E+1}^{qN_E} \left(\delta_{e2}^2 \check{h}_2^{i,m} + \delta_{e2}^2 \check{h}_2^{i,m} \right) \Phi_{i,l} h_1^i x_k + \tau_u, \quad (80) \end{aligned}$$

$$\begin{aligned} \check{y}_u^{RASSK} &= E_s \sum_{q=1}^{N_a} \sum_{i=(q-1)N_E+1}^{qN_E} \left(\delta_{e2}^2 \check{h}_2^{i,m} + \delta_{e2}^2 \check{h}_2^{i,m} \right) \Phi_{i,l} h_1^i + \tau_u. \quad (81) \end{aligned}$$